POLITECNICO DI MILANO

Master thesis in Material Engineering and Nanotechnology
Chemistry, Material and Chemical Engineering Department
"Giulio Natta"

Electrophoretic deposition of Bioglass/Chitosan Composites for bone tissue engineering applications

Supervisor: Prof. Luigi De Nardo
Co-Supervisor: Dr. Lina Altomare

Mehdi Soleimanzade
Matricola: 814876

Academic Year: 2015-2016

Acknowledgments:

I also desire to thanks my friends here specially Foad, Reza, Ashkan, Ali and Sogol who have been always giving me hope and support me in hard moments and giving me real taste of friendship.

Finally, I want to have special thanks to my beloved parents and brothers, for their endless supports and for their kind considerations and appreciations even from this far distance from my homeland Iran.

Mehdi

Table of Contents

Abbreviations

AA: Acetic Acid

BG: Bioglass

CH: Chitosan

EDS: Energy-dispersive X-ray spectroscopy

EPD: Electrophoretic Deposition

HA: Hydroxyapatite

HMI: Human Machine Interface

PBS: Phosphate Buffer Saline

SBF: Simulated Body Fluid

SEM: Scanning Electron Microscope

XRD: X-ray Diffraction analysis

List of Figures

List of tables

Abstract

Because of the advances in the scaffolds fabrication techniques, bone tissue engineering is increasingly becoming a method of choice for the development of viable substitutes for skeletal reconstruction. The scaffolds designed for bone tissue-engineering applications should be three-dimensional (3D), highly porous and interconnected to support cell attachment as well as proliferation. They should have sufficient structural integrity matching the mechanical properties of native tissue. They should provide suitable pore size distribution for transportation of nutrients and wastes. The scaffolds should offer ideal and critical micro-environment so that they can function as an artificial extra-cellular matrix (ECM) onto which cells attach, grow, and form new tissues. Most available scaffold fabrication methods, such as solvent casting, sol-gel, freeze drying are either limited to producing scaffolds with simple geometry, or depend on indirect casting method for scaffold fabrication. These traditional scaffold fabrication methods result in structures of random internal architecture.

Recently, it is proven that cells are inherently sensitive to their surroundings. The more the culturing environment of cell is similar to natural tissue the more the cell attachment and proliferation. For this, more biomimetic environments must be created. Various solid freeform fabrication (SFF) techniques including 3D printing, selective laser sintering, multi-phase jet solidification, and fused deposition modeling (FDM) have been used successfully to manufacture advanced tissue scaffolds with specific designed properties. The scaffolds manufactured using SFF

methods have 100% interconnectivity and the highly oriented porosity of these scaffolds can easily be controlled by optimizing the processing.

Electrophoretic deposition (EPD) is known to be one of the most effective and efficient techniques to assemble fine particles. This technique has received huge attention due to its simplicity in setup, low equipment cost and the capability to form complex shapes and patterns in room temperature. Recently, its application in biomedical area have also been widely explored. However, the feasibility of using EPD for fabricating scaffolds that can mimic the architecture of bone tissue and can be comparable with expensive SFF methods has not been investigated yet.

In this study, an attempt has done to survey on possibility of using (EPD) technique as a method to design and fabricate chitosan/Bioglass composite scaffolds mimicking the Haversian system of compact bone. Materials that were used in this study was chitosan and Bioglass 45S5®. Bioglass 45S5® is a well-known commercial composition of bioactive glasses with high bioactivity is proven to enhance formation of hydroxyapatite in physiological fluids and can be readily attached to the bone in relatively short time. However, it suffers from low mechanical properties. It is suggested to be composited by a high biocompatible hydrogel as a matrix or supporter. Derived from chitin, chitosan is a unique biopolymer that exhibits outstanding properties, beside biocompatibility and biodegradability. Most of these peculiar properties arise from the presence of primary amines along the chitosan backbone. As a consequence, this polysaccharide is a relevant candidate in the field of biomaterials, especially for tissue engineering.

In this regards, firstly parameters such as voltage, pH, Bioglass to chitosan ratio on quality of deposited composite has been explicitly investigated. Secondly, after optimizing the parameters, by exploiting oriented patterned porous aluminum

substrates with pore size similar to that of Haversian system, composite scaffolds with highly oriented microchannels has fabricated. Scanning electron microscope (SEM) images shows very good distribution of Bioglass particle embedded in chitosan matrix. In-vitro analysis shows dissolution of Bioglass particles in Phosphate Bovine Saline (PBS) solution. in Simulated Body Fluid (SBF), weight gain measurements and X-ray diffraction (XRD) analysis reveals the crystallization of a calcium phosphate dihydrate with formula $CaHPO_4.2H_2O$ which increases in amount and size by soaking time and also accompanying a small decrease in pH of SBF solution.

Sommario

Gli scaffold progettati per la rigenerazione del tessuto osseo dovrebbero essere tridimensionali (3D), altamente porosi e interconnessi per sostenere l'adesione cellulare e la proliferazione. Essi dovrebbero avere sufficiente integrità strutturale corrispondente alle proprietà meccaniche del tessuto nativo. Essi dovrebbero avere adeguata distribuzione delle dimensioni dei pori per il trasporto di sostanze nutritive e di scarto. Gli scaffold dovrebbero offrire un micro-ambiente ideale e critico in modo che possano funzionare come matrice extracellulare artificiale (ECM) su cui le cellule possano aderire, crescere e formare nuovi tessuti.

La maggior parte dei metodi di fabbricazione disponibili, come l'evaporazione da solvente, sol-gel, freeze drying sono o limitate a produrre scaffold con geometria semplice, o dipendono dallo stampo utilizzato. Queste metodi di fabbricazione tradizionali si traducono in strutture con architettura interna casuale.

Varie solide tecniche di fabbricazione prive di stampo (SFF), tra cui la stampa 3D, sinterizzazione laser selettiva, multi-fase di solidificazione del getto, e la modellazione a deposizione fusa (FDM) sono stati utilizzati con successo per la produzione di scaffold avanzati per l'ingegneria del tessuti proprietà specifiche. I scaffold realizzati con metodi SFF mostrano 100% di interconnettività e hanno una porosità altamente orientata che può essere facilmente controllata ottimizzando l'elaborazione.

La deposizione elettroforetica (EPD) è nota per essere una delle tecniche più efficaci ed efficienti per assemblare particelle fini. Questa tecnica ha ricevuto grande

attenzione grazie alla sua semplicità, il bassa costo delle apparecchiature e la capacità di creare forme complesse e modelli a temperatura ambiente. Recentemente, la sua applicazione in campo biomedico è stata ampiamente esplorato. Tuttavia, la possibilità di utilizzare EPD per la realizzazione di scaffold che possano mimare l'architettura del tessuto osseo, con risultati e paragonabili con costosi metodi SFF non è stato ancora studiata.

In questo studio, si è cercato di rilevare la possibilità di utilizzare la tecnica (EPD) come metodo per progettare e fabbricare scaffold compositi chitosano / Bioglass mimando il sistema Haversian dell'osso compatto. I materiali che sono stati utilizzati in questo studio sono chitosano e Bioglass 45S5®. Bioglass 45S5® è un noto prodotto commerciale composto da vetri bioattivi ad elevata bioattività capaci aumentare la formazione di idrossiapatite in fluidi fisiologici e di attaccarsi all'osso in tempi relativamente brevi. Tuttavia, possiede basse proprietà meccaniche. Si suggerisce di mescolarlo ad un altro idrogel biocompatibile come matrice o sostenitore. Derivato da chitina, il chitosano è un biopolimero unico che presenta proprietà eccellenti, tra cue accanto biocompatibilità e biodegradabilità. La maggior parte di queste proprietà peculiari derivano dalla presenza di ammine primarie lungo la catena del chitosano. Di conseguenza, questo polisaccaride è un ottimo candidato nel campo dei biomateriali, in particolare per l'ingegneria tissutale.

A questo proposito, in primo luogo parametri quali la tensione, il pH, il rapporta Bioglass/chitosano sulla qualità depositato è stato esplicitamente studiato. In secondo luogo, dopo l'ottimizzazione dei parametri, sfruttando substrati di alluminio con prosita orientate e con dimensioni dei pori simili a quella del sistema Haversian, sono stati fabbricati scaffold compositi con microcanali altamente orientati ha fabbricato. Le immagini ottenute con microscopio elettronico a scansione (SEM)

mostrano una molta buona distribuzione di particelle Bioglass incorporate nella matrice di chitosano. Analisi in vitro mostrano la dissoluzione delle particelle di Bioglass in soluzione salina (PBS). In soluzione fisiologica (SBF), le misurazioni del guadagno di peso e la diffrazione a raggi X (XRD) rivelano la cristallizzazione di fosfato di calcio diidrato con formula $CaHPO_4.2H_2O$ che aumenta in quantità e dimensioni in base al tempo di immersione che determina una piccola diminuzione della pH delle soluzione SBF.

Introduction

1.1. The need for tissue-engineered bone products

Restoration of bone defects in the different regions of body are often difficult, because of the complex three-dimensional structure and mechanical competence of damaged. Hence, it presents a significant challenge and is a focus of extensive basic, translational, and clinical research activity [1], [2]. Bone defects result from acute trauma, congenital abnormalities, on cological tissue resection, or progressive deforming diseases; they can range from the small, few millimeter periodontal defects, to the large, several centimeter segmental defects [1].

The treatment outcomes strongly depend on the size and location of the bone defects, surgical skills, and the quality of adjacent soft tissues, which are critical for graft vascularization and healing [3]. Particularly in large defects, the effects of osteoinductive signals rely on the presence of sufficient population of viable cells capable of forming new tissue, and appropriate vascular supply from the adjacent tissue, which might not be available in every patient [4].

The above-described shortcomings motivated research and development of new tissue engineering (TE) strategies to enhance bone repair in situations where conventional treatments fail. Developments in tissue culture technologies allow the ex-vivo cultivation of bone tissue substitutes tailored to match the anatomy of a specific patient's defect [5].

1.2. Strategies for tissue engineering of bone substitutes

TE bone substitutes are essentially designed to replicate the bone autograft functionality, with no or minimal additional injury to the patient, and with availability in quantities that are required for bone reconstructions. Various strategies have been developed that incorporate combinations of osteogenic cells, osteoinductive signals, and osteoconductive matrices or scaffolds [6]. In some cases, TE bone substitutes are also developed to enhance tissue vascularization, to improve the survival of cells in the bone defect, and to enhance integration and tissue remodeling [4]. Depending on where the new tissue formation takes place, the strategies can broadly be divided into *in-vivo* and *ex-vivo* tissue engineering [7], [8].

1.2.1. In vivo tissue engineering

In the in situ TE approach, scaffolds prepared from osteoconductive biomaterials are implanted in the bone defects, to fill the structural gap and provide support for new bone deposition by the ingrowing host cells. Scaffolds of various structures and chemistries are being developed and tested for their potential to stimulate new bone formation [9]. Ideally, the scaffolds should maintain structural integrity while they are gradually resorbed and replaced by the new tissue forming at the same rate. In order to enhance the bone repair processes, scaffolds can be combined with autologous bone or bone marrow grafts, or with osteoinductive factors at the time of implantation [10]. Alternatively, osteoinductive signals can be incorporated or conjugated to the scaffold material, to allow sustained release during scaffold resorption [11].

1.2.2. Ex-vivo tissue engineering

Ex-vivo TE is frequently used to prepare viable, cellularized bone substitutes [12]. Osteogenic cells are harvested, in most cases culture expanded to sufficient numbers, and seeded into scaffolds which are selected from a variety of porous, particulate or hydrogel biomaterials. For clinical TE, the scaffolds are often composed of biomaterials already approved for clinical use, such as hydroxyapatite ceramics, deproteinized bovine bone, processed bovine collagen, and synthetic polymers. The cell-seeded scaffold constructs are then cultured in-vitro in the presence of biochemical and biophysical stimulatory signals to promote osteogenesis [13].

1.3. Bone structure and properties

Bone is a hard tissue found in living systems, which serves both as mechanical support and as mineral reservoir in the body. It has remarkable mechanical properties, with Young's moduli spanning a large spectrum of stiffness (10^1 MPa to 10^2 GPa) and a highly anisotropic structure [14]. The main source of complexity in bone arises from the fact that bone is a hybrid nanocomposite, where inorganic hydroxyapatite (HA, $Ca_{10}(PO_4)_6(OH)_2$) nanoplatelets orient and regularly disperse within the triple helix structure of collagen fibrils. Different suprafibrillar arrangements of collagen fibrils further result in hierarchical structures spanning several length scales [15]. To fulfill various clinical applications in TE and implanting, researchers have attempted for decades to reproduce in the laboratory this complex hierarchical structure, hoping to achieve a material capable of truly mimicking real bone [16].

3

As with all organs in the body, bone tissue has a hierarchical organization over length scales that span several orders of magnitude from the macro- (centimeter) scale to the nano-structured (extracellular matrix or ECM) components figure 1-1. Bone ECM comprises both a nonmineralized organic component (predominantly type-1 collagen) and a mineralized inorganic component (composed of 4 nm thick plate-like carbonated apatite minerals) [17]. In addition, over 200 different types of noncollagenous matrix proteins (glycoproteins, proteoglycans, and sialoproteins) contribute to the abundance of signals in the immediate extracellular environment. The nano-composite structure (tough and flexible collagen fibers reinforced by hydroxyapatite, HA, crystals) is integral to the requisite compressive strength and high fracture toughness of bone [18].
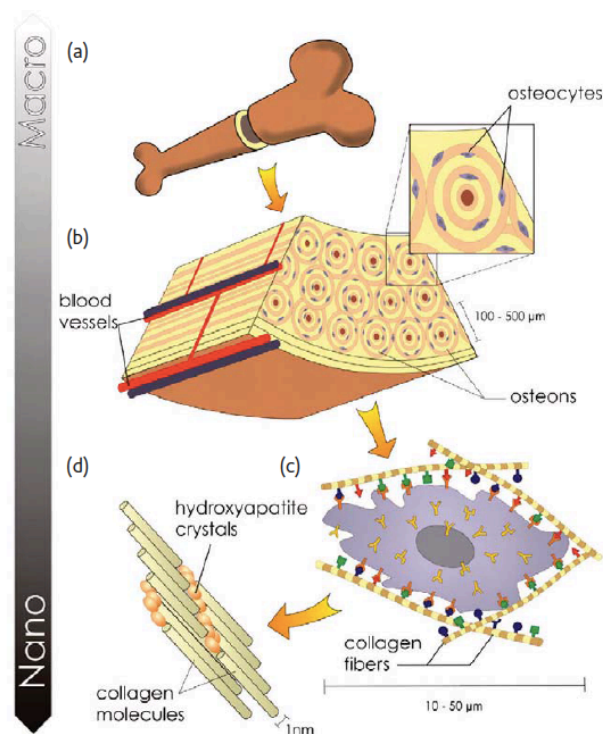
Figure 1-1: Hierarchical organization of bone over different length scales. Bone has a strong calcified outer compact layer (a), which comprises many cylindrical Haversian systems, or osteons (b). The resident cells are coated in a forest of cell membrane receptors that respond to specific binding sites (c) and the well-defined nano architecture of the surrounding extracellular matrix (d) [18].

4

1.4. Biomaterial Scaffolds

Osteoconductive scaffolds provide a three-dimensional structural and logistic template for the developing bone tissue substitute, and therefore markedly affect the behavior of implanted as well as in-growing cells. Cell survival, attachment, migration, proliferation, and bone formation are affected by the scaffold structure, mechanical properties, and chemistry, including the size, shape, and distribution of pores, roughness and specific nano-features of scaffold surfaces, and the presence of specific chemical groups and attachment sites [19]. Scaffolds must provide appropriate bone-like mechanical stiffness, allow nutrient and waste transport, and support vascularization and integration with the surrounding tissue. In addition, for the successful development of TE bone products, scaffolds must provide processibility into selected shapes, and ease of sterilization and implantation [19].

As a result of these complex requirements, there is no ideal biomaterial scaffold for all clinical situations [20], and a variety of scaffolds are being tested in the development of TE bone products [10], [19]. For instance, in-vitro and preclinical in vivo studies showed that scaffolds from metals, ceramics, naturally derived and synthetic polymers, and composite materials support new bone formation. In clinical studies, natural and synthetic bone scaffolds resembling the mineral phase of bone and with mechanical stiffness appropriate to support new tissue deposition, such as coral-derived hydroxyapatite [21] and synthetic hydroxyapatite with/without beta-tricalcium phosphate [12], [22], [23] were frequently used. In addition, biocompatible synthetic polymers, which have a lower mechanical competence but offer the possibility of processing into various structures, were also used to prepare TE bone products [24].

1.5. Biomaterials for bone repair

While materials intended for implantation were in the past designed to be 'bioinert', materials scientists have now shifted toward the design of deliberately 'bioactive' materials that integrate with biological molecules or cells and regenerate tissues [25], [26]. In the case of bone, materials should preferably be both osteoinductive (capable of promoting the differentiation of progenitor cells down an osteoblastic lineage), osteoconductive (support bone growth and encourage the ingrowth of surrounding bone), and capable of osseointegration (integrate into surrounding bone). Many bone substitute materials intended to replace the need for autologous or allogeneic bone have been evaluated over the last two decades. In general, they consist of either bioactive ceramics, bioactive glasses, biological or synthetic polymers, and composites of these [25], [27], [28]. The ideal basic premise, if following the tissue engineering paradigm, is that the materials will be resorbed and replaced over time by, and in tune with, the body's own newly regenerated biological tissue [26].

1.5.1. Bioactive inorganic materials

A wide range of bioactive inorganic materials similar in composition to the mineral phase of bone are of clinical interest, e.g. tricalcium phosphate, HA, bioactive glasses, and their combinations (figure 1-2) [25],[28]. Bioactive glasses (Ca- and possibly P-containing silica glasses), for example, when immersed in biological fluid, can rapidly produce a bioactive hydroxycarbonated apatite layer that can bond to biological tissue. Furthermore, they can be tailored to deliver ions such as Si at levels capable of activating complex gene transduction pathways, leading to enhanced cell differentiation and osteogenesis [25], [29], [30]. The brittle nature of bioactive

inorganic materials means that their fracture toughness cannot match that of bone and on their own are not good for load-bearing applications. Apart from hydroxyapatite (HA) implants, one of the conditions for ceramic materials (CM) to be bioactive is to form a HA layer on their surfaces while exposed to simulated body fluid (SBF).

The mechanism of HA formation on bioactive silica-based CM has been studied by different authors [31]. All of them claim that a silica hydrogel layer is formed on the surface of the CM prior to the formation of the HA layer. This hydrated silica is responsible for the HA nucleation.
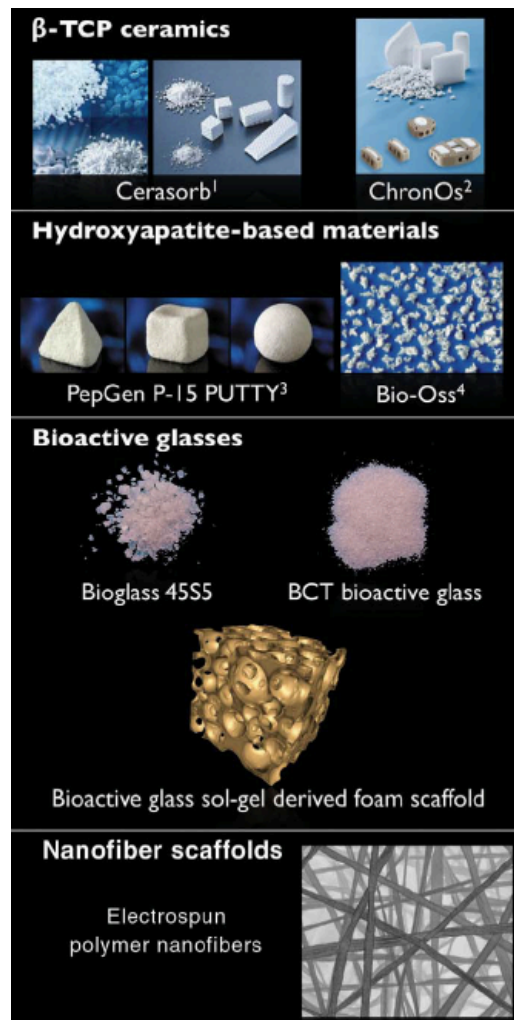
Figure 1-2: Macromorphology of some examples of different bone graft materials [18].

The original bioactive glass 45S5® has been used as a baseline for most surface studies, largely because it is single phase and has only four components (Na_2O, CaO, P_2O_5, SiO_2). This simple composition also has the highest in vivo bioactivity index (I_B), introduced by Hench [47] as $I_B=100/t_{0.5bb}$, where $t_{0.5bb}$ is the time for more than 50% of the implant interface to be bonded to bone. Table 1-1 shows the sequence of HA formation from Bioglass [31].

Table 1-1: Reaction Stages of a Bioactive Implant [31]

Stage	Reaction
1	Rapid exchange of Na^+ or K^+ with H^+ or H_3O^+ from solution: $Si\text{-}O\text{-}Na^+ + H^+ + OH^- \rightarrow Si\text{-}OH^+ + Na^+(solution) + OH^-$ This stage is usually controlled by diffusion and exhibits a $t^{-1/2}$ dependence.
2	Loss of soluble silica in the form of $Si(OH)_4$ to the solution, resulting from breaking of Si-O-Si bonds and formation of Si-OH (silanols) at the glass solution interface: $Si\text{-}O\text{-}Si + H_2O \rightarrow Si\text{-}OH + OH\text{-}Si$ This stage is usually controlled by interfacial reaction and exhibits a $t^{1.0}$ dependence.
3	Condensation and repolymerization of a SiO_2-rich layer on the surface depleted in alkalis and alkaline-earth cations: $$\begin{array}{ccccc} O & O & O & O \\ \mid & \mid & \mid & \mid \\ O\text{-}Si\text{-}OH + HO\text{-}Si\text{-}O \rightarrow O\text{-}Si\text{-}O\text{-}Si\text{-}O + H_2O \\ \mid & \mid & \mid & \mid \\ O & O & O & O \end{array}$$
4	Migration of Ca^{2+} and PO_4^{3-} groups to the surface through the SiO_2-rich layer forming a $CaO\text{-}P_2O_5$-rich film on top of the SiO_2-rich layer, followed by growth of the amorphous $CaO\text{-}P_2O_5$-rich film by incorporation of soluble calcium and phosphates from solution
5	Crystallization of the amorphous $CaO\text{-}P_2O_5$, film by incorporation of OH^-, CO_3^{2-}, or F^- anions from solution to form a mixed hydroxyl, carbonate, fluorapatite layer.

1.5.2. Hydrogels

Hydrogels are three-dimensional networks composed of hydrophilic polymers cross-linked either through covalent bonds or held together via physical intramolecular and intermolecular attractions. Hydrogels can absorb huge amounts

of water or biological fluids, up to several thousand %, and swell readily without dissolving. The high hydrophilicity of hydrogels is particularly due to the presence of hydrophilic moieties such as carboxyl, amide, amino, and hydroxyl groups distributed along the backbone of polymeric chains. In the swollen state, hydrogels are soft and rubbery, resembling to a great extent the living tissues. In addition, many hydrogels, such as chitosan and alginate-based hydrogels show desirable biocompatibility [32].

Hydrogels usually reach their equilibrium swelling when a balance occurs between osmotic driving forces, which encourage the entrance of water or biological fluids into the hydrophilic hydrogel matrix, and the cohesive forces exerted by the polymer strands within the hydrogel.

There are two big families of hydrogels: Natural and Synthetic.

1.5.2.1. Natural polymers-based hydrogels for tissue engineering:

Several hydrogels have been developed from natural polymers for tissue engineering applications. These natural polymers include for instance, polynucleotides, polypeptides, and different polysaccharides. They are obtained from a variety of natural origins; for example, chitosan is obtained from shellfish exoskeletons whereas, collagen is obtained from mammals.

Chiosan, β-(1-4)-linked D-glucosamine (deacetylated unit) and N-acetyl-D-glucosamine (acetylated unit), is the only amino polysaccharide distributed in large amounts in nature It is the deacetylated derivative of chitin, the most abundant natural polymer on earth after cellulose, obtained from crustaceans, such as shrimps, squids, and crabs. Chitosan has been used in many industries including wastewater treatment, medicine, food, and cosmetics [32].

In general, hydrogels based on polymers from natural origins, such as chitosan, are advantageous in tissue engineering applications due to their intrinsic characteristics of biological recognition, including presentation of receptor-binding ligands and the susceptibility to cell-triggered proteolytic remodeling and degradation. However, the use of natural component-based hydrogels has shown some drawbacks, which involve the complexities associated with purification, immunogenicity and pathogen transmission.

1.5.2.2.   Synthetic polymer-based hydrogels for tissue engineering

Hydrogels based on natural polymers have demonstrated many shortcomings including the difficulty of purification, immunogenicity and pathogen transmission. Although some of these shortcomings can be overcome, greater control over material characteristics and tissue responses are achievable when using hydrogels based on synthetic analogs [33].

Although all of these properties of hydrogels made them a promising biomaterial candidate for tissue engineering, due to lack of bioactivity they can not be used alone for bone tissue engineering.

1.5.3. Bioactive glasses reinforced by hydrogels

A drawback of bioactive glasses, and more general in ceramics, is their low fracture toughness and mechanical strength, especially in a porous form. Hence, bioactive glasses alone have limited application in load-bearing situations [34]. It can be seen that particularly porous scaffolds needed for tissue engineering exhibit very low mechanical properties compared to cortical and cancellous bone.

Development of composite scaffold materials is attractive as advantageous properties of two or more types of materials can be combined to suit better the mechanical and physiological demands of the host tissue. By taking advantage of the formability of polymers and including controlled-volume fractions of a bioactive ceramic phase, mechanical reinforcement of the fabricated scaffolds can be achieved [35]. At the same time, the poor bioactivity of most polymers can be overcome.

Probably the most important driving force behind the development of polymer/bioactive glass composite scaffolds for bone tissue engineering is the need for conferring bioactive behavior to the polymer matrix, which is achieved by the bioactive inclusions or coatings. The degree of bioactivity is adjustable by the volume fraction, size, shape and arrangement of inclusions [36] [37]. It has been shown that increased volume fraction and higher surface area to volume ratio of inclusions favor higher bioactivity, hence in some applications the incorporation of fibers instead of particles is favored [38].

Moreover, the scaffolds should have appropriate and controllable mechanical properties, e.g. elastic constants and compressive strength, thus providing temporary support for cells to enable tissue regeneration [39].

Inclusion of bioactive glasses has been shown to modify surface and bulk properties of composite scaffolds by increasing the hydrophilicity and water absorption of the hydrophobic polymer matrix, thus altering the scaffold degradation kinetics. In particular, the inclusion of 45S5 Bioglasss particles was found to increase water absorption compared to pure polymer foams of PDLLA [40] and PLGA [41]. Ideally, the degradation and resorption kinetics of composite scaffolds are designed to allow cells to proliferate and secrete their own

extracellular matrix while the scaffolds gradually vanish, leaving space for new cell and tissue growth. The physical support provided by the 3D scaffold should be maintained until the engineered tissue has sufficient mechanical integrity to support itself [24].

1.6. Technologies to fabricate composite materials for bone tissue engineering

In recent years, considerable attention has been given to the development of fabrication methods to prepare porous ceramic scaffolds for osseous tissue regeneration. The ideal fabrication technique should produce complex-shaped scaffolds with controlled pore size, shape and orientation in a reliable and economical way. However, all porous materials have a common limitation: the inherent lack of strength associated with porosity. Hence, their application tends to be limited to low-stress locations, such as broken jaws or fractured skulls. Therefore, the unresolved dilemma is how to design and create a scaffold that is both porous and strong [42].

1.6.1. Infiltration of bio-ceramics phase with the polymer phase

The basic process developed to fabricate both polymer coated inorganic scaffolds and polymer–ceramic scaffolds with interpenetrating network microstructures consists of infiltrating a sintered or partially sintered bioceramic scaffold with the polymer phase [43], as schematically shown in figure 1-3. In most cases, a biodegradable synthetic polymer is used.
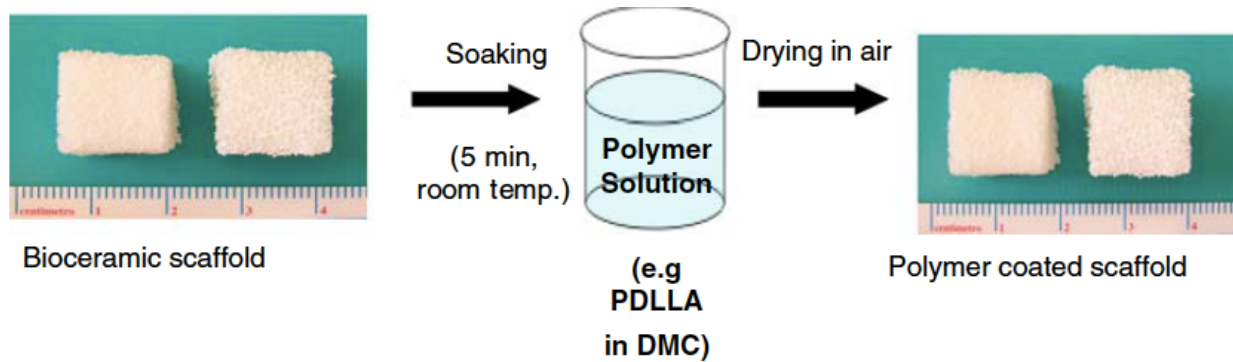
Figure 1-3: Polymer solution dipping method developed to coat bioceramic scaffolds with biodegradable polymers, e.g. PDLLA solution in dimethyl carbonate (DMC) [44].

The open micropores of the struts were infiltrated with poly(lactic-co-glycolic acid) (PLGA) to achieve an interpenetrating bioactive ceramic/biodegradable polymer composite structure. This work followed from earlier work by M. Yunos et al. [44], where PLGA-coated porous CPC scaffolds were developed exhibiting compressive strength values of up to 4 MPa. In their most recent investigation Miao et al. [45] further coated the PLGA filled struts with a 58S bioactive glass (33 wt%) PLGA composite coating. The resulting scaffolds proved to be bioactive and exhibited even higher compressive strength values (up to 7.7 MPa) and compressive moduli of up to 3 GPa, these values being comparable to those of natural spongy bone.

1.6.2. Freeze-drying of composite solution

Freeze casting is a simple technique to produce porous complex-shaped ceramic or polymeric parts [46]. In freeze casting, a ceramic slurry is poured into a mold and then frozen. The frozen solvent acts temporarily as a binder to hold the part together for demolding. Subsequently, the part is subjected to freeze drying to sublimate the solvent under vacuum, avoiding the drying stresses and shrinkage that may lead to cracks and warping during normal drying. After drying, the compacts are sintered in

order to fabricate a porous material with improved strength, stiffness and desired porosity. The result is a scaffold with a complex and often anisotropic porous microstructure generated during freezing. By controlling the growth direction of the ice crystals, it is possible to impose a preferential orientation for the porosity in the final material [47].

There is the possibility of blending the biocompatible polymers with bio active ceramics in a solution and fabricate a three dimensional composite scaffold by freeze drying the solution. For instance, Sultana et al. produced three-dimensional composite scaffolds with controlled microstructures and an interconnected porous structure by blending two biodegradable and biocompatible polymers, namely poly(hydroxybutyrate-co-hydroxyvalerate) (PHBV) and poly(L-lactic acid) (PLLA) with incorporated nano hydroxyapatite using an emulsion freezing/freeze-drying technique figure 1-4 [48].
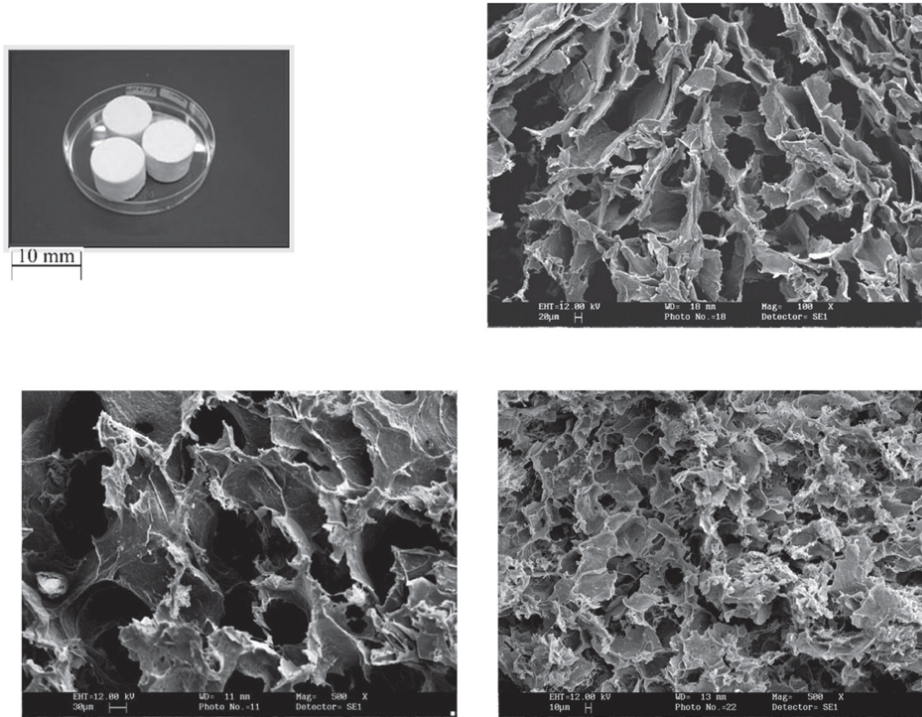
Figure 1-4: Scaffolds fabricated using the emulsion freezing/freeze-drying technique: (a) physical appearance; (b), (c), (d) SEM micrographs of scaffolds of different compositions [48].

14

HA nanoparticles were homogeneously dispersed in the polymer matrix, which is one of the advantages of this fabrication route. Amount and particle size distribution of ceramic particles, concentration of the polymers, solvent, freeze drying temperature and pressure are the main factors regarding the final composite structure [49].

1.6.1. Sol-gel technique

A century of sol-gel science has seen its founding with the discovery of room-temperature hydrolytic routes to silica glasses and its diversification into technologies for the preparation of highly structured nano to macroporous inorganic and hybrid organic-inorganic polymers with an astounding range of chemistries [49].

The steps for making macroporous sol-gel-derived bioactive glasses, termed bioactive foams, and their characterization for physical properties are shown in figure 1-5.
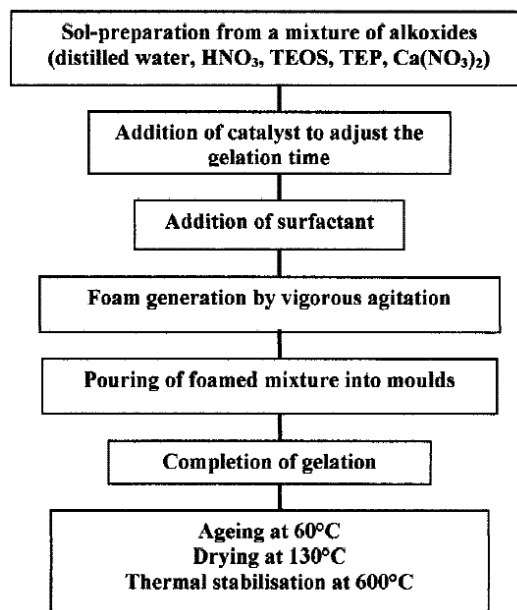
Figure 1-5: Schematic representation of the manufacture of sol-gel foams [50].

The glasses can be manufactured with specific architectures to obtain controlled rates of glass resorption and rates of chemical dissolution of species that promote tissue regeneration, thus creating a novel three–dimensional tissue construct similar to natural tissues. A range of potential applications is possible for the repair and reconstruction of diseased and damaged tissue, as matrices for graft implant materials, or as devices for the controlled release of biologic or pharmaceutical substances [50].

Wang et al. [51] developed a new porous bioactive nanocomposite composed of sol–gel-derived bioactive glass nanoparticles (BG), collagen (COL), hyaluronic acid (HYA) and phosphatidylserine (PS) by a combination of sol–gel and freeze-drying methods. They also synthesized a bioactive nanocomposite by crosslinking collagen and HYA by using 1-ethyl-3-(3-dimethylaminopropyl) carbodiimide (EDC) and N-hydroxysuccinimide (NHS). After crosslinking, the structure of BG–COL–HYA–PS scaffolds became more ordered and channel pores preferentially aligned. The scaffolds were seen to be highly porous with pore size in the range 100–400 μm. It was reported that bio-mineralization and degradation in SBF, and mechanical strength of the EDC/NHS-crosslinked BG–COL–HYA–PS composite scaffolds were better than those of the scaffolds without HYA, PS, and crosslinking process. PS and HYA play an important role in the regulation of the bio-mineralization process, inducing HA to precipitate on the surface of the composites.

Mansur et al. report the development and characterization of novel hybrid macroporous scaffolds of poly(vinyl) alcohol (PVA)/bioactive glass (BaG) through the sol–gel route. The organic–inorganic hybrids with three concentrations of PVA (80, 70 and 60 wt%) and bioactive glass ($58SiO_2$–$33CaO$–$9P_2O_5$) were synthesized by foaming a mixture of polymer solution and bioactive glass via sol–gel precursor

solution. PVA with two degree of hydrolysis, 98.5% (high degree) and 80% (low degree) was also investigated, in order to evaluate the influence of residual acetate group present in polymer chain on the final structure and properties of 3D porous nanocomposites produced (PVA/BG) [52].

1.6.2. Electrophoretic deposition (EPD) technique

Bioceramic-coated porous scaffolds have been produced either as foams [53], fibrous bodies [54] or meshes [55] by electrophoretic deposition (EPD). EPD appears as a versatile, simple and low cost technique to create highly homogeneous coatings with clear advantages, like the possibility to obtain homogeneous coatings on 3D structures of complex shape as well as on porous substrates in room temperature [56]. Moreover, EPD enables production of a wide variety of coatings due to the possibility of depositing different types of materials and combination of materials, like inorganic, polymeric and composite materials with high microstructural homogeneity and tailored thickness [57]. The EPD process is based on the application of an electric field between two conductive electrodes immersed in a colloidal suspension. The electric field imparts electrophoretic motion to charged particles in suspension causing their movement to the oppositely charged electrode, where they deposit forming a coherent coating over it [58]. EPD is usually carried out in a two electrode cell, as schematically shown in figure 1-4 [59].
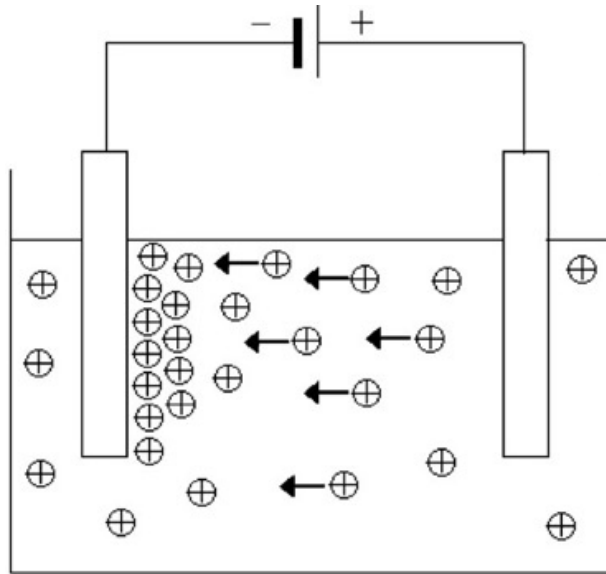
Figure 1-6: Two electrodes cell for electrophoretic deposition showing positively charged particles in suspension migrating towards the negative electrode [59].

The mechanism of electrophoretic deposition involves two steps. In the first step an electric field is applied between two electrodes and charged particles suspended in a suitable liquid move toward the oppositely charged electrode (electrophoresis). In the second step the particles accumulate at the deposition electrode and create a relatively compact and homogeneous film (deposition). In order to effectively apply this technique to process materials, it is essential to produce a stable suspension containing charged particles free to move when an electric field is applied. Therefore EPD can be applied to any solid that is available as a fine powder (e.g. <~30 μm particle size) or as a colloidal suspension, including metals, polymers, ceramics and glasses [60]. Parameters effecting EPD is shown in table 1-2.

Table 1-2: Parameters governing EPD

Suspension parameters	Process parameters
Particle size	Applied electric field
Dielectric constant, conductivity and viscosity	Deposition time
Zeta potential	Conductivity of the substrate
Stability	
Concentration of solids	

1.6.2.1.   Effect of Applied Electric Field

As there are both intended particles and free ions in the suspension, a portion of the electric field, which is the driving force of EPD, is carried by the free ions and the field efficiency is compromised. However, when we cannot limit the presence of free ions, the amount of current carried by them is insignificant. Ideally, the applied electric field must be totally spent on advancement of the electrophoresis in a stable-current manner, because the deposition increases in direct relation with raising the applied potential. While too low fields are not capable of triggering the electrophoresis, with too high applied electrical fields, the quality of the deposits is sacrificed. It has been suggested that the best quality of deposits is gained at moderate applied fields. Moreover, a high electric field can cause turbulence in the suspension, which compromises the quality of the resulting deposit. Also, it increases the speed of the particles and consequently they cannot have the chance to be seated in the best position, which makes the formation of a dense close-packed structure impossible [61].

1.6.2.2.   Effect of Deposition Time

In EPD, the deposition rate starts with a linear relationship to time and then it lowers as time goes on, until the deposit is thick enough to interrupt the conductance and the deposition rate reaches plateau at high deposition times.

1.6.2.3.   Conductivity of Substrate

In EPD, the quality of the deposited film is strongly dependent on the conductivity of the substrate. Low conductivity of the substrate leads to both slow deposition and nonuniformity of the deposit [62].

In the last 20 years the interest in electrophoretic deposition as a technique to produce advanced materials has widely increased, both in academia and in the industrial sector, and since then a wide range of new applications of EPD for processing a variety of bulk materials and coatings has been reported [59].

For example, EPD has been utilized to deposit materials with improved wear and oxidation resistance, and to produce functional coatings for electronic, magnetic and to deposit bioactive coatings for biomedical implants related applications [58].

The EPD mechanism of chitosan macromolecules has been explained by Zhitomirsky and co-workers [63]. It is suggested that the protonated amine-groups of chitosan (figure 1-7) lose their charge in the high pH region at the cathode surface to form an insoluble deposit. In solution, the salt form of chitosan dissociates to polycations with a charge that depends on its molecular weight and deacetylation degree (DA) as well as on negatively charged counterions.
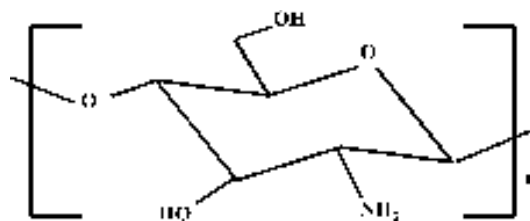
Figure 1-7: Chemical structure of chitosan [63].

Mechanism of codeposition of Chitosan/Bioglass has explained by Pishbin et al. [64] according to overlapping of the FTIR spectra of Chitosan/Bioglass bands with those of the chitosan structure. They showed that the suspension of glass particles

in aqueous medium leads to formation of free surface hydroxyl groups which can be involved in hydrogen-bonding with chitosan hydroxyl and carbonyl moieties. This hydrogen-bonding results in adsorption of chitosan on glass particles, provides their electrosteric stabilization in the suspension and in turn aids the co-deposition of the glass and polymer components.

Co-deposition of polymers and ceramics is one of the most interesting features of EPD applied to the development of biomaterials [65]. Recently, EPD of chitosan/vancomycin antibiotic[66] and chitosan/nanobioactive glass/ampicilin antibiotic as drug releasing coatings have been investigated. In another study Patel et al.[67] have demonstrated EPD of chitosan-gelatin composites loaded with ampicillin as a model drug and have achieved a rate-controllable drug release by a compositional change in the polymers ratio of the deposited films. EPD have also been used to coat stainless steel cardiovascular stents: one study involves EPD of rapamycin-loaded mesoporous silica nanoparticle/carbon nanotube composite30 and the other has shown EPD of N-nitro-somelatonin-loaded poly(D,L-lactide-co-glycolide) nanoparticles [68].

1.7. Mimicking the bone tissue structure using modern technologies

Traditionally, materials design, while considering bulk tissue properties, has not encompassed the entire spectrum of biological length scale topography known to influence cell behavior (ranging from 10 nm to 100 μm).

Recently, it is proven that cells are inherently sensitive to their surroundings. Topographic reaction (i.e. reaction to the surface landscape) of cells to grooves, ridges, wells, and other features at the micron scale. For this, more biomimetic environments must be created[69].

Several attempts have been done for mimicking the bone tissue structure using modern technologies such as electron beam lithography (EBL) [70] and also fused deposition modeling (FDM) [71] which allow the development of manufacturing processes to create porous scaffolds that mimic the microstructure of living tissue (figure 1-8 and 1-9).

There are now numerous examples of biological and synthetic polymer electrospun three-dimensional nanofiber matrices with high spatial interconnectivity, high porosity, and controlled alignment to direct cell orientation and migration. These scaffolds may even be directly mineralized by introducing P-containing anionic functional groups into the backbone of the polymers or as pendant groups to induce the nucleation and deposition of HA [69].
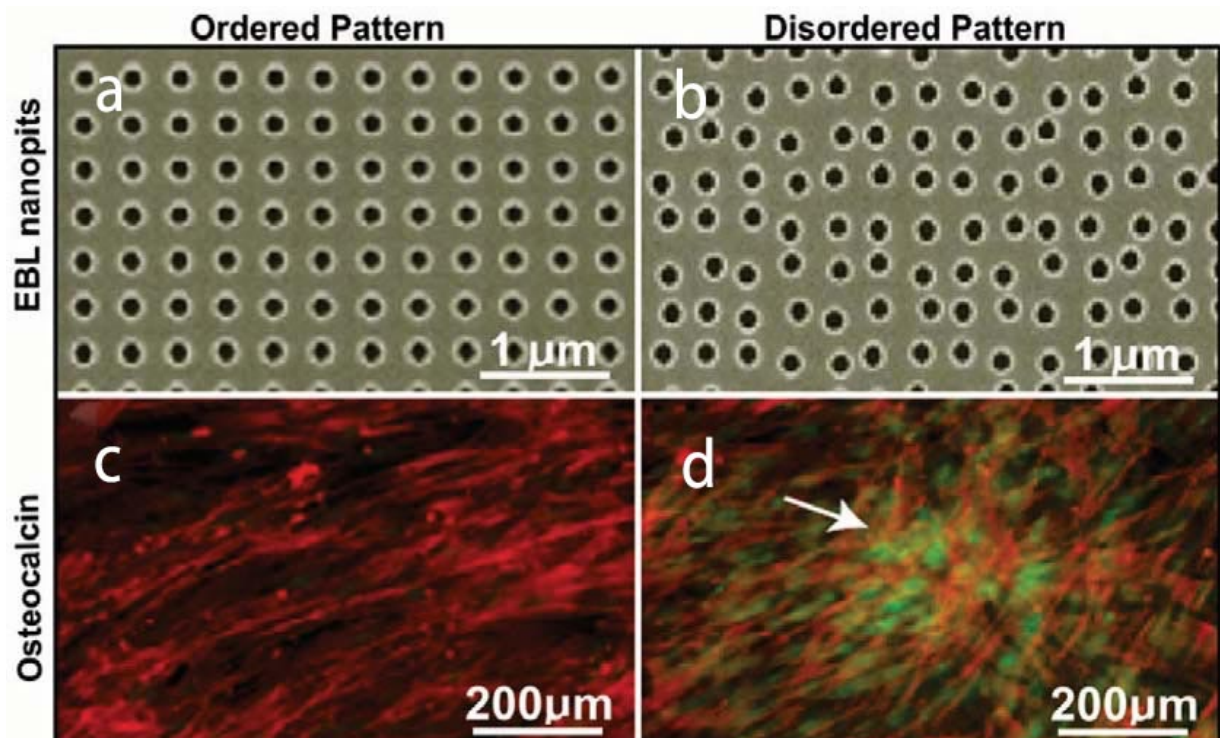
Figure 1-8: Exploring the effect of different nanotopographies on cell differentiation. (a, b) Nanotopographies of increasing disorder were fabricated by electron beam lithography (EBL). The pits (120 nm in diameter and 100 nm deep) were generated (a) in a square arrangement and (b) with increasing disorder (displaced square ±50 nm from true center). The nanoscale disorder

stimulates human mesenchymal stem cells to increase the expression of the bone-specific ECM
protein osteopontin (d, arrow) compared with the ordered structure (c) [70]
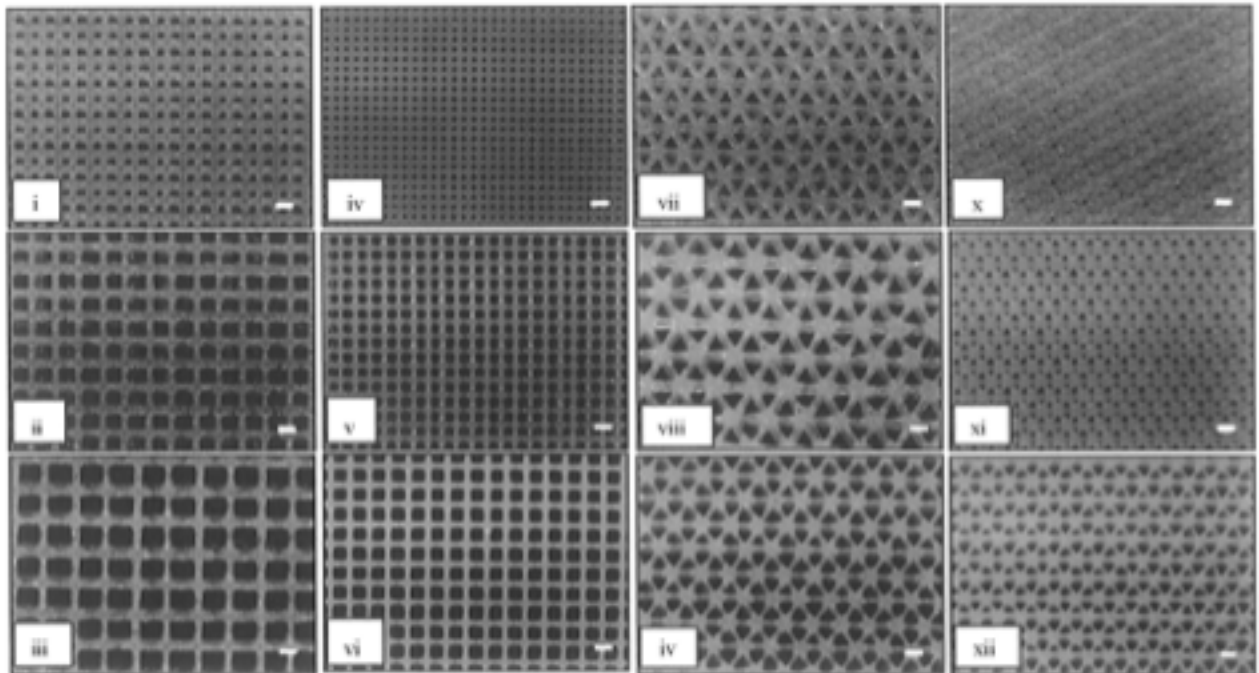
Figure 1-9: 3D scaffold systems of various porosity and pore geometry fabricated by FDM [71]

Aim of Work

The use of EPD for the fabrication of patterned scaffolds that mimic the exact structure of the target tissue has been less considered.

In this study firstly, we optimize the parameters affecting a uniform deposition of Chitosan/Bioglass composite scaffold and secondly deposit the composite on a patterned cathode with similar porosity size of the osteon. In this case there would be a scaffold with high bioactivity and also exact shape and microchannels of Haversian system as the target tissue to be implanted.

Electrophoretic deposition (EPD) is chosen as the fabrication route, as it is a room temperature and very cheap technique in which deposition properties can be effectively tuned by deposition parameters such as pH and voltage. In addition, complex architectures can be realized homogenously. 45S5 Bioglass® powder with two size distributions and chitosan, a natural polysaccharaide (85% deacetylated), are used as the source materials for producing a polymer matrix with bioactive glass composite. Furthermore, patterned aluminum templates with different pore size are exploited to produce samples which can resemble, as close as possible, the structure of the osteon.

Moreover, to study the response of the samples in physiological-like environments, best samples are soaked in SBF and PBS up to 28 days of incubation time. Water uptake and weight gain of samples are measured during the test. Further investigations proceed using characterization techniques such as XRD, SEM, EDS. By XRD, probable crystallized calcium phosphate phases will be investigated.

SEM and EDS are used to survey the microstructure of possible crystalline phases and also homogeneity of embedded Bioglass into the Chitosan matrix.

2. Material and methods

2.1. 45S5 Bioglass

45S5 Bioglass is one of the most important formulations of a commercially available family of bioactive glasses. It was developed by professor L. Hence [31]. It's a melt-derived glass consisting of:

45% of SiO_2 (Silicon dioxide)

6% P_2O_5 (Phosphorous oxide)

24.5% of CaO (Calcium oxide)

24.5% of Na_2O (Sodium oxide)

The name "45S5" refer to both SiO_2 content (45%) and CaO/P_2O_5 molar ratio (5).

In this study we used 45S5 glass with two different size distribution. Large size Bioglass that were used in this study was provided by Dr. L.P. Lefebvre from Laboratorio di Neurofisiologia del CNR, Pisa. Small size Bioglass was provided by Prof. Aldo R. Boccaccini from Institute for Biomaterials, University of Erlangen-Nuremberg in Germany.

2.2. Chitosan

Electrophoretic deposition was performed using medium molecular weight chitosan (MMW chitosan, Aldrich 448877, Lot SLBH2747V) with a deacetylation degree higher than 75%.

It was dissolved in water-based (Aldrich Chromasolv Plus®) acetic acid (AA) solutions in different pHs (5 to 3).

2.3. Electrophoretic cell structure

1. Anode: Two graphite rods (ϕ = 6.3 mm and length ≈ 20 cm) were used as anodes

2. Cathodes: Table 2-1 shows the type of metal substrate used as cathode in electrophoretic cell.

3. Plastic beaker

4. Nitrogen diffuser system

5. Stirrer

6. Keithley multimeter (model 2425 100W SourceMeters®)

7. LabVIEW (National InstrumentTM)

8. Black and red wires to connect the interface to the cathode and anode respectively.

Table 2-1: Materials, dimensions and hole sizes of strips used as cathode in EPD

Material	Dimensions (mm)	Channel size (mm)	Pore center to center distance (mm)
AISI 316L Stainless Steel	20 x 40 x 1.0	N/A	N/A
Aluminum Anticorodal Bar En Aw 6026	20 x 40 x 1.0	0.5	0.9
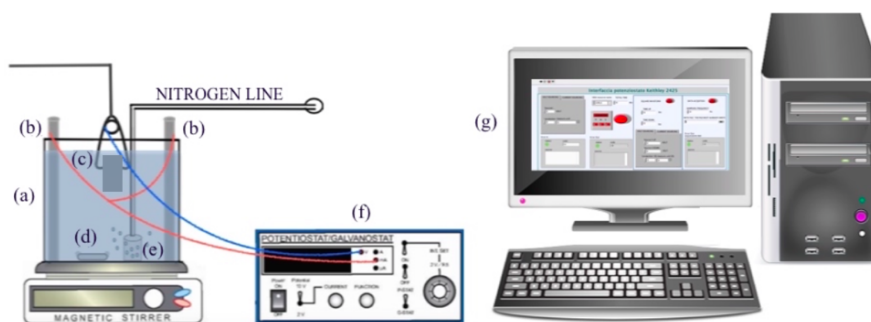
Figure 2-1: The electrophoretic cell is composed by: (a) a plastic beaker, (b) two graphite anodes, (c) one cathode, (d) a magnetic stirrer, (e) a nitrogen diffuser. Anodes and cathode are connected to the power supply (f) by a red and blue wire, respectively. A computer interface (g) set current and voltage parameters and acquire data [72].

2.4. Design of process

2.4.1. Production of Bioglass-Chitosan composite samples by EPD

Electrophoretic deposition was performed using medium molecular weight chitosan (MMW chitosan, Aldrich 448877, Lot SLBH2747V) with a deacetylation degree higher than 75%. It was dissolved in different water-based (Aldrich Chromasolv Plus®) acetic acid (AA) solutions at different pHs (3.0, 3.2 and 3.5 etc. and concentration = 1.0 g.L^{-1}). Before deposition process the electrolytic solution's pH and conductivity were measured with Hach HQ11d portable pH/ORP Meter and Crison CM 35 portable conductimeter respectively. Mentioned graphite rod was used as anode and metal plates as cathodes. The distance between the graphite rods and the cathode was fixed at 3.5 cm. Except an area of 1cm x 1cm all cathode surface was carefully insulated with Kapton insulating tape.

Before deposition process the electrolytic solution's pH and conductivity were carefully measured. The deposition process was performed with a Keithley multimeter (model 2425 100W SourceMeters®).

LabVIEW (National InstrumentTM) was exploited to develop an Human Machine Interface (HMI) between computer and multimeter. This interface allows to set the digital multimeter, it is possible to select galvanostatic or potentiostatic control of the EPD process and the applied value. Moreover, the user can choose to set constant current/voltage or square waveforms with whichever duty cycle. Finally, it is possible to acquire and save real time current and voltage values in the electrolytic cell.

Prepared electrolytic solution is poured into in the electrophoretic cell shown in figure 2-2.

After degassing for 1 hour with nitrogen (N_2), EPD was performed up 20 minutes at room temperature. Multimeter was connected to electrodes and input sequence was programmed by HMI to investigated only in potentiostatic conditions:

• potentiostatic mode: voltage values were fixed to provide 25, 50 or 75 V. Different square waveforms were also tested with duty cycle of 50% or 16% and with fixed value of maximum and minimum voltage (100 and 75 V) [72].
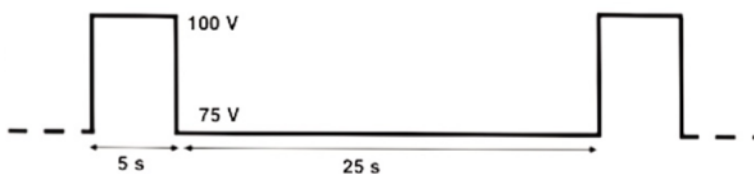
Figure 2-2: Square waveforms with 16% of duty cycle tested in potentiostatic [72].

At the end of EPD, samples were immersed in 0.1 M NaOH solution for 1 min in order to remove all AA residues that can possibly be on chitosan surface and then were consecutively immersed in 3 becker with distilled water to remove all reagents. After that the samples were put in oven (37°C) for at least 4 hours or put in freeze-dryer (5Pascal model Lio 5P 230V) for 24 hours to let them dry. The BG-CS composite films were manually peeled off the cathode metal substrate by forceps.

2.4.2. Deposition on micro-patterned cathode as positive master via EPD

Micro-patterned aluminum substrates were used in order to verify if through EPD it is possible to replicate porosities of the templates. These porosities are to mimic the structure of osteon. Figure 2-3 shows SEM image of aluminum grids with 500μm diameter of oriented porosities.

The cathodes dimension and channel sizes were listed in table 2-1. All parts of patterned aluminum substrate were insulated using Kapton wire except the gridded parts in both sides. In this case two graphite rods were fixed in both sides of the

cathode templates in the solution, with anode to cathode distance of 3cm. In this case, for each time of deposition both sides of cathode were coated at the same time. Other procedure was exactly the same as section 3.4.1.
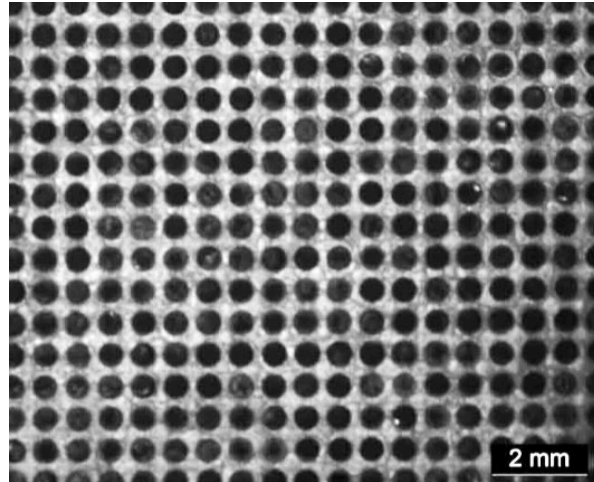
Figure 2-3: SEM observation of aluminum grids with 500µm oriented pore size.

Dried samples were cut into circular shape with 7mm diameter using a punch. Following samples were used in Simulated Body Fluid (SBF) and Phosphate-Buffered Saline (PBS) tests.

2.4.3. In-vitro tests

The bioactivity of scaffolds was investigated by immersion in SBF and PBS solutions (pH 7.4 at 37 °C) for 1, 2, 7, 14 and 28 days. The SBF solution was prepared, following Kokubo et al. [73]. Each sample (with the dimensions of 7 mm in diameter) was placed in new 24-well x 4mL multi-dish cell cluster (flat bottom with lid, non pyrogenic polystyrene strile corning™ incorporated).

The samples ware coded and put into the wells. After the solutions reaches 37°C, 4 milliliters of SBF and PBS were added to each sample by micropipette. Three of each sample family for every time step were used. Multiwall was sealed by paraffin to avoid evaporation of solutions.

Multi-dish cells swung very slowly on a flip-flopper instrument all in oven (temperature set at 37°C).

For every time steps the residual solutions were drawn and frozen for pH and conductivity evaluations.

After extraction from solution, every sample was washed with large amount of Millipore-water, wet weighted and then lyophilized for at least 24h, weighted and stored in vacuum for next analysis.

All the multi-dish cells were kept in an incubator at 37°C and every two days the solution extracted completely and exchange with fresh solution.

2.4.3.1.   Simulated Body Fluid (SBF)

The Simulated body fluid is a solution containing different salts that simulate the concentrations and pH of human blood plasma and is able to reproduce in-vitro the in vivo apatite formulation. In fact, Kokubo concluded that "a material able to have apatite formation on its surface in SBF can bond to living bone through apatite layer formed on its surface in the living body, as long as the material does not contain any substance induces toxic or antibody reactions"[74].

- Procedure for 1 liter SBF preparation:

900 mL Millipor water was used and pour in to a Plastic beaker. The beaker was washed very carefully. Beaker with the stirrer and magnet was put inside the oven at 37°C. Because, during the whole procedure the temperature must be kept at 37°c. The salts were added to the solution in the order the Table 2-2 one at a time:

Aluminum foil was used to avoid contaminants enter it when left the solution in the oven. Final pH must be exactly 7.4. Rest of the H2O -which is also at 37°C- was added to solution to reach 1 liter SBF. Final solution was cooled down to room

temperature and then kept it in closed Plastic bottle in fridge. If needed, filter was used to remove possible impurities.

Table 2-2: The salts that should be added one by one for SBF preparation.

	Reagent	Quantity
1	NaCl	8,035 gL^{-1}
2	NaHCO3	0,355 gL^{-1}
3	KCl	0,225 gL^{-1}
4	K2HPO4 * 3H2O	0,231 gL^{-1}
5	MgCl2 * 6H2O	0,311 gL^{-1}
6	HCl (1 M)	39 mL
7	CaCl2	0,292 gL^{-1}
8	Na2SO4	0,072 gL^{-1}
9	Tris	6,118 gL^{-1}
10	HCl (1 M)	Drops to establish the final pH

2.4.3.2.   Phosphate-Buffered Saline (PBS)

Phosphate-buffered saline (PBS) is a buffer solution used in biological research. It is a water-based salt solution containing sodium phosphate, sodium chloride and, in some formulations, it contains potassium chloride and potassium phosphate. The osmolality and ion concentrations of the solutions match those of the human body (isotonic) and are non-toxic to most cells [75].

- Procedure for 1 liter PBS 1X preparation:

Table 2-3: Reagents needed for 1X and 10X PBS preparation

Reagent	1X solution (g)	Final Conc. 1X (mM)	10X solution (g)	Final Conc. 10X (mM)
NaCl	8	137	80 g	1370
KCl	0.2	2.7	2 g	27
Na2HPO4	1.44	10	14.4 g	100
KH2PO4	0.24	1.8	2.4 g	18

PBS can be made as a 1X solution or as a 10X stock. To prepare 1 liter of either 1X or 10X PBS, the reagents listed in Table 2-3 should be dissolved in 800 mL of H2O.

The pH should be adjusted to 7.4 with HCl, and then H2O is added to 1 liter. The solution is dispensed into aliquots and is sterilized by filter sterilization. PBS is stored at room temperature.

2.4.4. Sample preparation

Table 2-4 shows the seven families of samples used for in-vitro analysis. The pore size of the patterned substrates was 500μm with pore center to center distance 900μm (figure 2-3). The pH of all solution were fixed at 3.00. All samples were deposited in square voltage condition (100-75V and 5-25s) for 1200 seconds. After depositions all the samples were washed carefully, lyophilized and then punched into circular shape with diameter of 7 mm.

In order to draw error bars and perform other statistical analysis. Therefore, there is 42 samples for each step time, 1, 2, 7, 14 and 28 days. Total number of 42 x 5= 210 samples are used for water uptake and weight gain analysis.

Table 2-4: Six different sample families for in-vitro analysis

Abbreviation	Preparation Solution composition	Substrate
CH	1 gL^{-1} Chitosan	Stainless steel, flat
CH-P	1 gL^{-1} Chitosan	Aluminum, Patterned
CH-10BGL	0.1 gL^{-1} Bioglass large size, 1 gL^{-1} Chitosan	Stainless steel, flat
CH-10BGL-P	0.1 gL^{-1} Bioglass large size, 1 gL^{-1} Chitosan	Aluminum, Patterned
CH-10BGS	0.1 gL^{-1} Bioglass small size, 1 gL^{-1} Chitosan	Stainless steel, flat
CH-10BGS-P	0.1 gL^{-1} Bioglass small size, 1 gL^{-1} Chitosan	Aluminum, Patterned
CH-30BGS-P	0.3 gL^{-1} Bioglass small size, 1 gL^{-1} Chitosan	Aluminum, Patterned

3. Results and Discussion

3.1. Fabrication process and results obtained by changing parameters

First part of the project is devoted to optimize the parameters affecting the quality of the deposited composites. The parameters that is chosen to be studied were the amount of Bioglass, pH of the solution, and voltage and also size distribution of the Bioglass powder.

The detail of these analyses are coming in following pages.

3.2. Morphological and size distribution of the powders

Two different grain size Bioglass 45S5 selected to be used as bioactive part of the composites. Figure 3-1 show the SEM image of the two powders. From these images, one can roughly estimate that the small grain size powder has average size of 3µm and large grain size one has mean size value of 30µm.
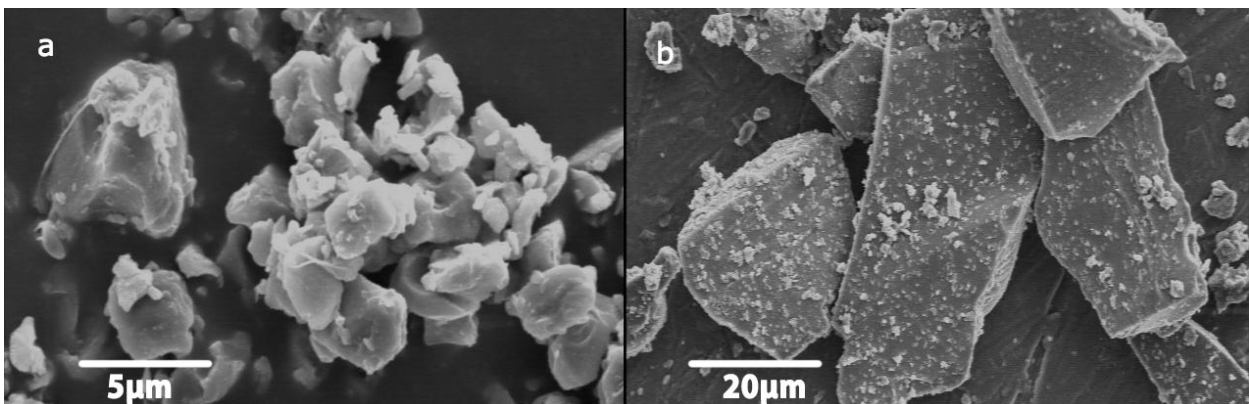
Figure 3-1: SEM images of a) small grain size and b) large grain size Bioglass 45S5

Table 3-1: EDS analysis of Pure Bioglass

Spectrum	O	Na	Al	Si	P	Ca	Total
Pure BG 45S5®	46.55	12.60	0.00	19.58	2.09	19.17	100.00

3.3. Study the effect of different parameter on deposition rate

Deposition rate is an important parameter affecting the quality of the final deposition. Slow deposition rate is not economically favorable and very fast deposition rate results in defects which lower the quality and homogeneity of final samples. In this case effect of three important parameters, Voltage, pH and Chitosan to Bioglass ratio, on the deposition rate has been evaluated as follow.

3.3.1. Effect of Voltage

As mentioned in part 1.6.4, applied bias between the anode and cathode is the driving force for particle flow towards the opposite electrode. Therefore, if we fix other parameters, by increasing the voltage, the deposition rate should be increased.

figure 3-2 shows the deposited weight versus time for 30, 50 and 75 volts. The composition of the solution was 0.1 gL-1 Bioglass and 1.0 gL-1 Chitosan. The pH of solution for three experiments was 4.21. Weight of samples was measured up to 600 seconds.
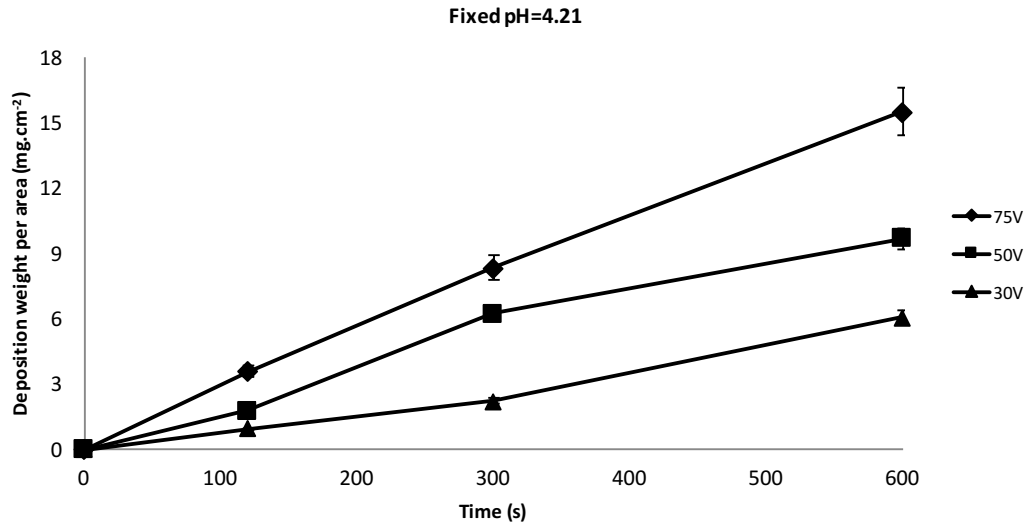
Figure 3-2: Deposition weight vs time for CH-10BG samples, pH fixed by acetic acid at 4.21

Up to 600 seconds there is linear relationship between time and weight. Moreover, deposition rate, slope of the graphs, increasing by increasing the voltage (figure 3-3).
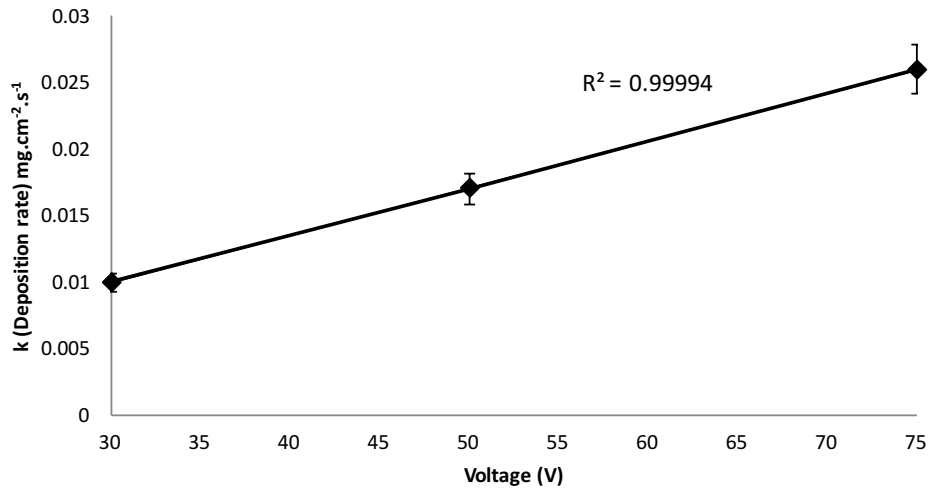
Figure 3-3: Linear relationship between deposition rate and voltage for CH-10BG samples

As proposed by Simchi et al. [76], the deposition rate k for chitosan (without any other component) can be expressed by the following equation:

$$k = \frac{FZ\varphi}{6\pi\eta r\rho}(E - \Delta E)$$ *Equation 1*

where μ is the electrophoretic mobility of the macromolecules, Z the electric charge and η the viscosity of the liquid, E is the electric field, ΔE the possible electric potential drop over the electrodes, ρ the density of the film and φ is the concentration. F is a correlation factor that takes into account that not all macromolecules brought to the electrode are incorporated in the deposit (F≤1).

From this formula which is valid only for short times and low concentrations (Newtonian flow) there is linear correlation between k and applied voltage. Figure 3-3 shows the trend of deposition rate for each voltage. R-square value of the graph is 0.9994 and this confirms this linear relationship. This graphs reveals that there exists linear relationship also for solutions contain small amount of Bioglass and Chitosan for short times, 0.1 g.L^{-1} BG and 1g.L^{-1} chitosan.

3.3.2. Effect of pH

For evaluating the effect of pH on deposition rate of BG/CH composite, a solution contains 0.1 gL^{-1} BG and 1.0 gL^{-1} CH was prepared and then by adding AA deposition weight over time up to 1200 seconds for different pHs have measured. Figure 3-4 shows the variation of deposited weight over time for the pHs 3.0, 3.3, 3.7.
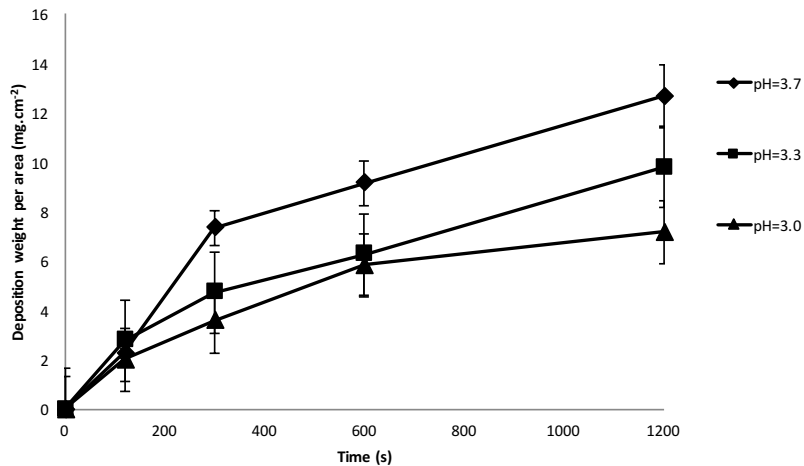
Figure 3-4: Effect of pH on deposition weight of the CH-10BGL samples

37

As can be seen, there are two regimes of deposition; up to 400 seconds there is a linear relationship between deposition weight and time but as the time elapses, due to shielding effect of deposited composite layer, rate of deposition start to decreases and will reach zero value in longer times, where the deposition stops.

Figure 3-5 shows the variation of solution conductivity by changing pH by AA.
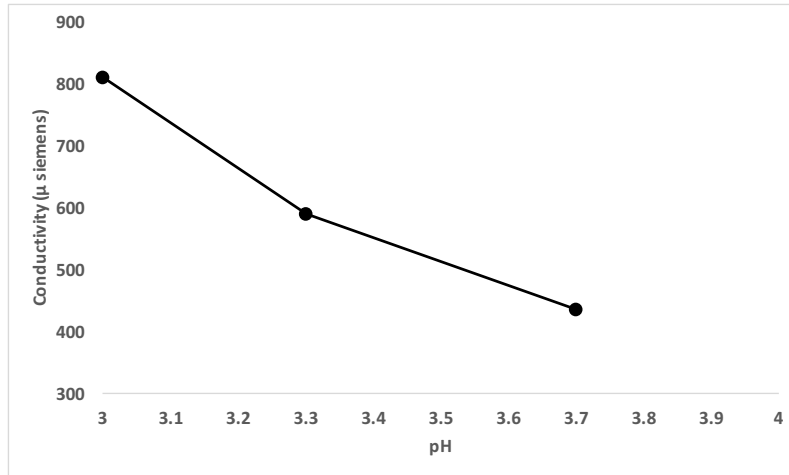
Figure 3-5: Conductivity versus pH of CH-10BGL solutions.

Deposited layer acts as an insulator and reduce the effective electric field E at the deposited surface. According to the Equation 1, when ΔE increases the deposition rate will decrease to the zero value.

As can be seen in figure 3-5 by decreasing the pH, conductivity of solution increases. Conductivity is a measure of ion concentration in the solution. When ion concentration increases, mobility of the chitosan molecules decreases. Therefore, the higher the pH, the lower the deposition rate.

Meanwhile, the EPD of chitosan in aqueous solution is accompanied by cathodic reduction of water and production of hydrogen gas at the cathode surface. Therefore, when the growth rate is relatively low, a dense film is formed. However, at higher growth rates the gas entrapment in the growing film causes pore formation, which should be avoided if dense film is desired [76].

3.3.3. Effect of Bioglass to Chitosan ratio

To study the effect of Bioglass to Chitosan ratios on deposited weight over time three different ratios BG:CH (wt% BG in solution/wt% CH in the solution) of 10, 1 and 0.5 were selected. Figure 3-6 shows the graphs related to these ratios in which the pH was 5, with constant voltage 75.
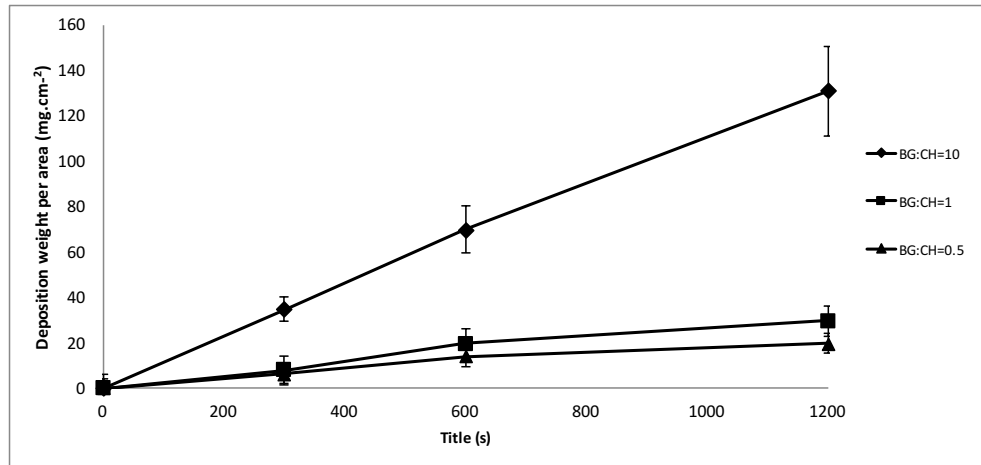
Figure 3-6: Deposition weight versus time for the solutions with Bioglass to chitosan different ratios (10, 1 and 0.5)

According these graphs shown in figure 3-6, there is a sudden increase in the deposition weight of the ratio 1 to 10. But, we can not consider the deposition yield of these solutions by this graph. Because unlike previous graphs, total available particles in the suspension is not fixed and it is changing by changing the ratio between the Bioglass and chitosan. To eliminate this effect, it is necessary to divide the deposition weight to total BG+CH amount added to the solution.

Percentage of deposition = (Deposited weight/sum of BG and CH weights) x 100   Equation 2

New graph (figure 3-7) will be the percentage of deposited weight to total suspended particles available in the solution. From this graph, it can be seen that there is not a big difference in the percentage of deposition yield of ratio 10:1 compared to ratios 1:1 and 0.5:1. This shows that by increasing 10x the Bioglass

particles in the solutions, only few of them are co-deposited with chitosan on the cathode surface. This observation proves very low deposition yielding of Bioglass particles. It is because of higher density of BG compared to CH, the density of 45S5 Bioglass® is 2.7 $g.cm^{-3}$ and density of chitosan is 0.6 $g.cm^{-3}$, and its deposition rate is much less than chitosan. Hence, even in solutions with high amount of Bioglass particles, chitosan is the prominent deposition in cathode and can make a polymeric matrix even in high ratios [64]. However, at very high BG concentrations, enough amount of CH was not deposited to provide a uniform matrix for BG embedment.

On the other hand, it should be noted that the samples with ratio 10:1 are too brittle to be used as scaffold.
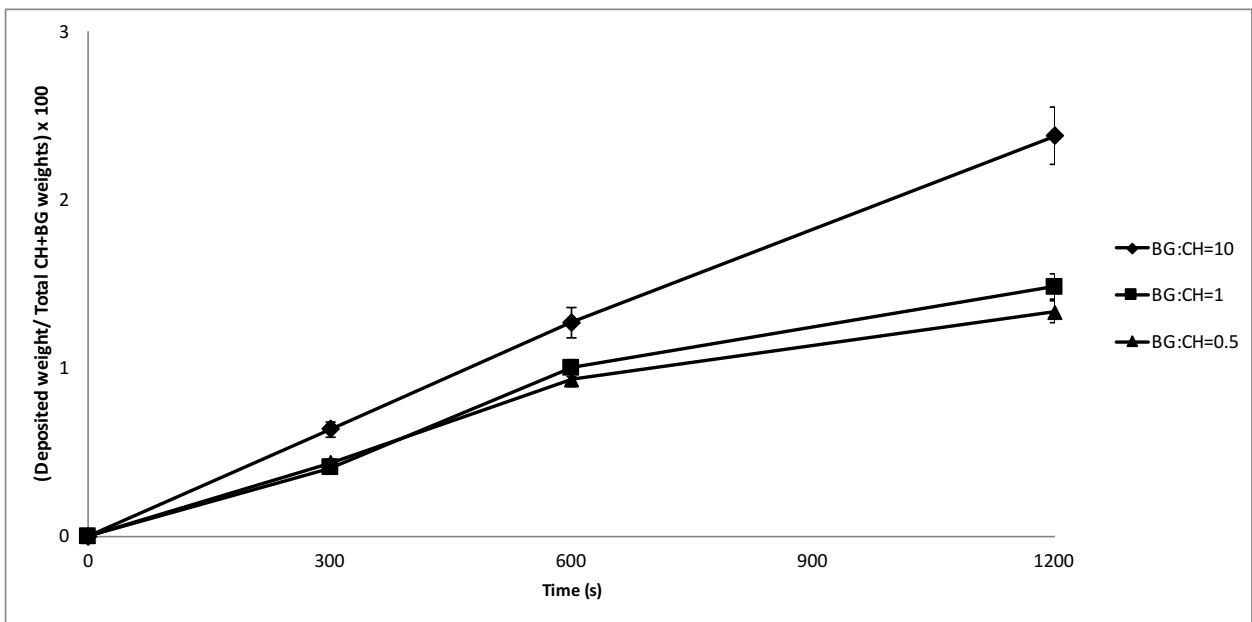
Figure 3-7 Percentage of deposited weight to the total weight of added components (Chitosan and Bioglass) to the solution

3.3.4. Effect of BG:CH ratio on quality of composite

The higher the amount of Bioglass the higher bioactivity of the scaffold. Thus, we started with BG to CH ratio 1:1. The resulting was a massive unstable gel-like covering at the cathode. There was no attachment of deposition to the cathode and

it was impossible to form and extract it with desired shape. These situation was the same for pHs 5 to 3. At lower pHs due to very high amount of conductivity (hundreds of μ Siemens) the solution reaches the boiling temperature after some minutes. According to these observations we decided to decrease the amount of BG to moderate the conditions. By decreasing the BG:CH ratio, gel-like structure changes into a more compact film with less overheating problems. But the gel-like problem of deposition didn't solve until the ratio was decreased to 0.3:1. Gel-like deposition on cathode surface is sown in figure 3-8 for the ratio 1:1.
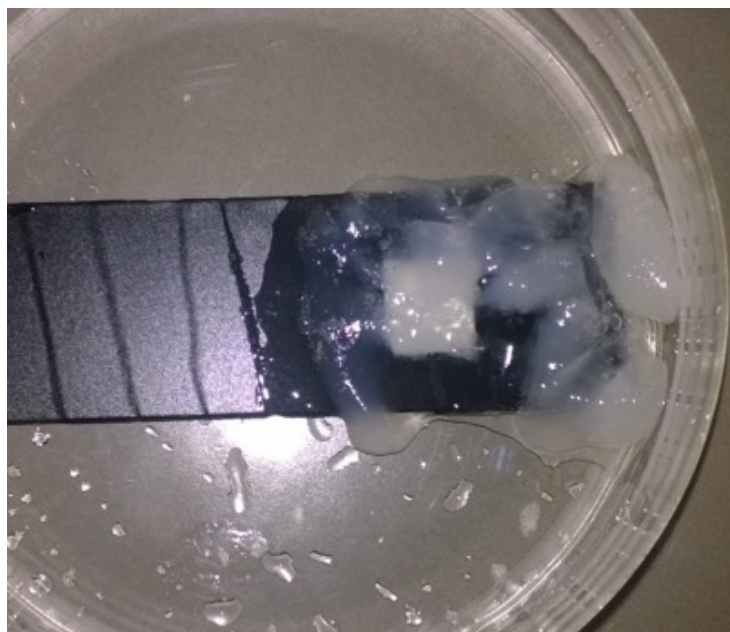
Figure 3-8: Gel-like deposition of Bioglass to Chitosan ratio 1:1 at pH=4, constant voltage 75, after 5 min.

For the ratio 0.1:1, there was a dense deposition with perfect attachment of the depositions to the cathode substrate. Figure 3-9 shows the stereoscope image of sample CH-10BGL after peeled off the cathode metal substrate and freeze-drying.
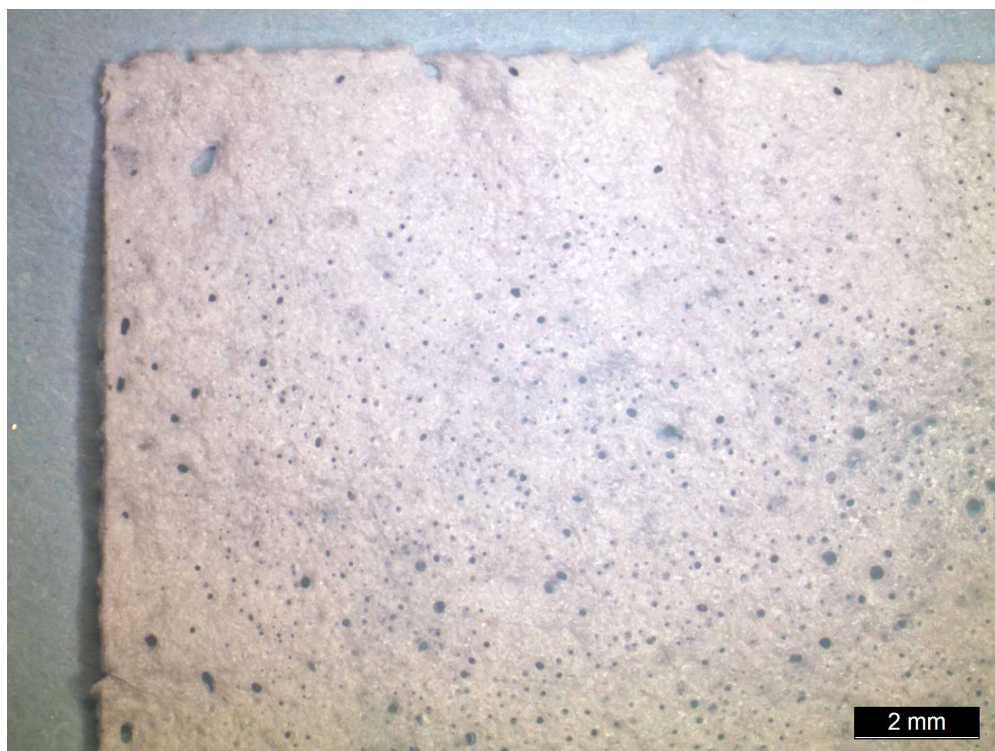
Figure 3-9: Stereoscope image of lyophilized CH-10BGL sample

CH is insoluble in water and in organic solvents. However, the protonated CH can be dissolved in water, water–ethanol and water–methanol mixtures at low pH. The protonation of the amine groups of CH can be achieved in acidic solutions:

$Chit\text{-}NH_2 + H_3O^+ \rightarrow Chit\text{-}NH_3^+ + H_2O$
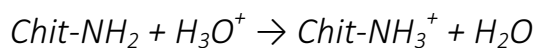
It is suggested that protonated CH loses its charge in the high pH region at the cathode surface and forms an insoluble deposition [77]:

$Chit\text{-}NH_3^+ + OH^- \rightarrow Chit\text{-}NH_2 + H_2O$
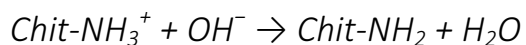
As mentioned in section 1.6.4., CH molecules attach to the Bioglass particles through hydrogen bonding and then carry the particles to the cathode where deprotonation of chitosan polycation is occurred. One possibility of gel formation is that BG particles reduce the tendency of chitosan deprotonation and this cause the gel-like form deposition.

However, investigating on exact mechanism of this phenomenon needs more precise rheological analysis which is beyond the scope of this research.

3.3.5. Effect of pH on the quality of deposition

Effect of pH on the quality of deposition was done on the sample with BG:CH ratio 0.1:1. This time deposition was performed on patterned aluminum cathodes with hole diameter of 500 μm and hole center to center 900 μm in order to evaluate the ability of the deposition to form exactly around these artificial ordered porosities. We start with pH of 3.7 and then start to decrease the pH. Because according to the results shown in figure 3-4, by decreasing the pH, deposition rate decreases. Hence, not only particles can find a longer time to deposit at the appropriate positions (around the holes) but also there will be less turbulence at the cathode surface and denser film with less defects would be deposited. In addition, hydrogen bubbles find more time to escape from the deposition without forming big porosities in the deposited film. The only draw back is that the lower the pH the longer the deposition time. Figure 3-9 shows depositions CH-10BGL-P samples performed at pHs 3.7, 3.3 and 3.0 right after the deposition.
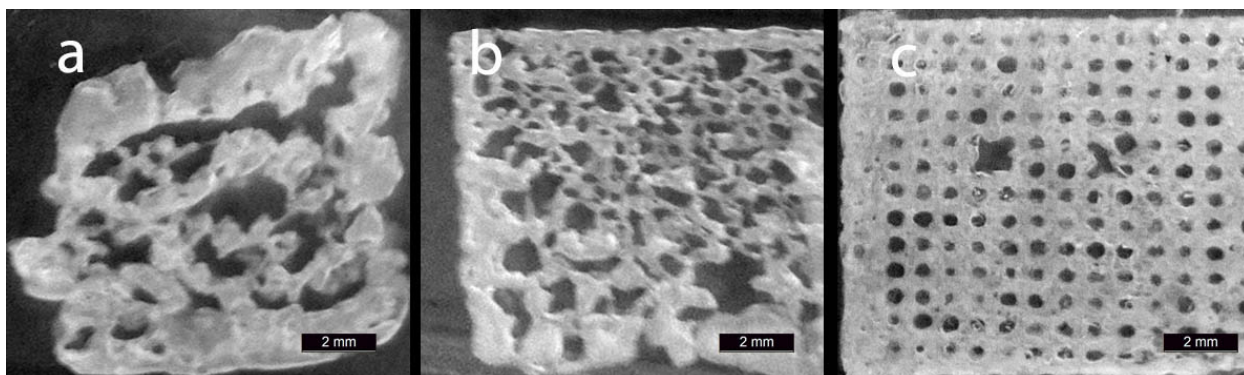
Figure 3-10: Optical observation of deposition at pH a)3.7 b)3,3 c) 3.0 from the CH-10BGL-P samples at square voltage (75-100V, 25-5s) after 20 min

Also, figure 3-11 and figure 3-12, shows the stereoscope and SEM images of highly oriented micro-channels of CH-10BGL-P sample deposited in pH 3.0 for 20 min, respectively. Big holes are the replication of patterned cathode and small holes are the result of hydrogen evolution at cathode surface through the following reaction [78]:

$$2H_2O + 2e^- \rightarrow H_2 + 2OH^-$$
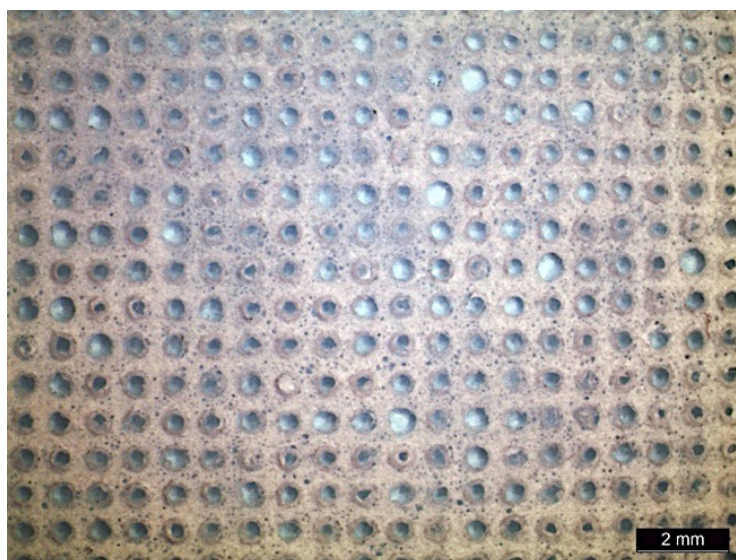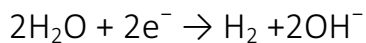
Figure 3-11: Stereoscope image of lyophilized CH-10BGL-P sample

Due to the small size of BG particles (figure 3-1), for observing the embedded Bioglass particles, higher magnifications is needed. Figure 3-13 shows the SEM image of figure 3-12 samples but in higher magnifications.

Bright spots in the image is the BG particles, because these images were taken in backscattered mode. Due to heavier elements in Bioglass compare to chitosan matrix, they shine like stars in polymer black background. It can be seen that Bioglass particles embedded very homogeneously in the CH matrix.
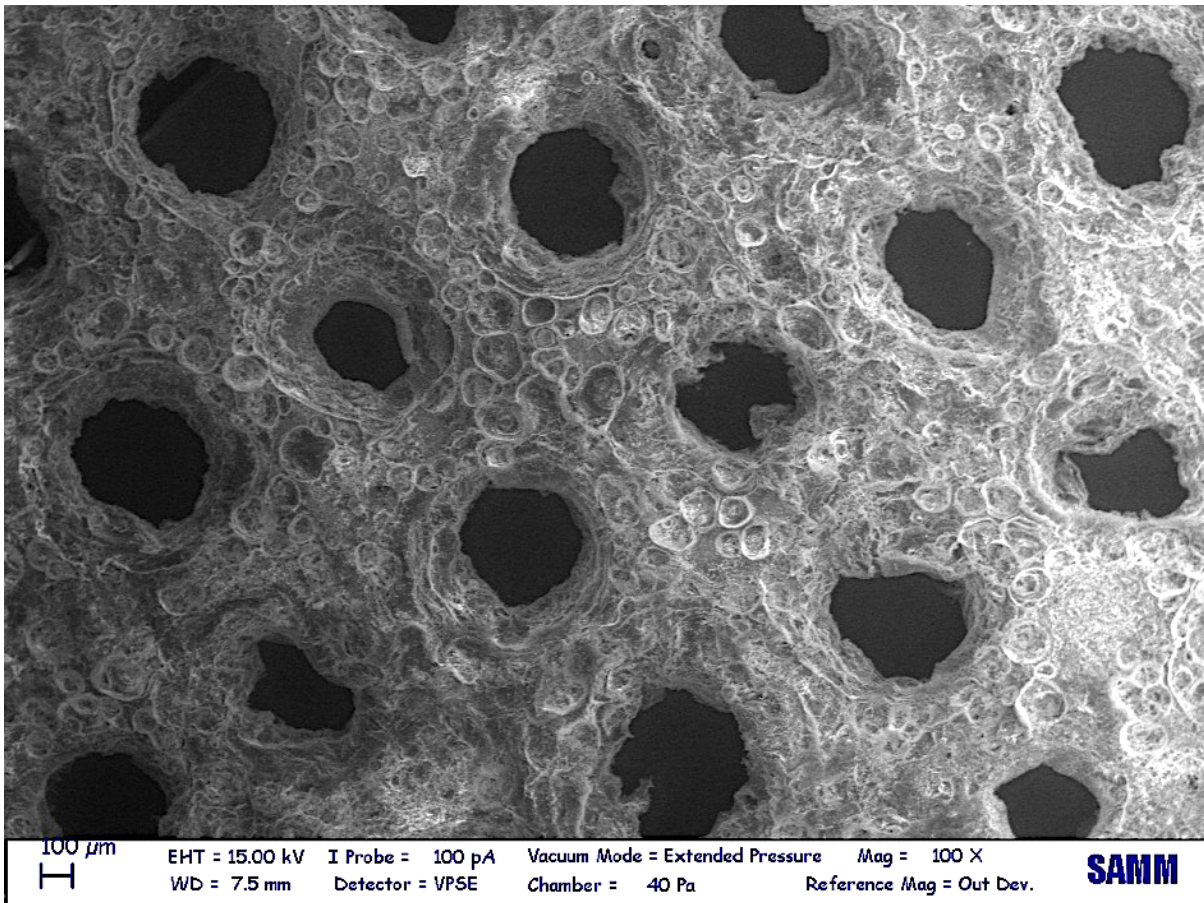
Figure 3-12: Secondary SEM image of highly oriented micro-channels of 10% Bioglass samples, prepared at pH 3.0 with square voltage (75-100V, 25-5s) after 20 min
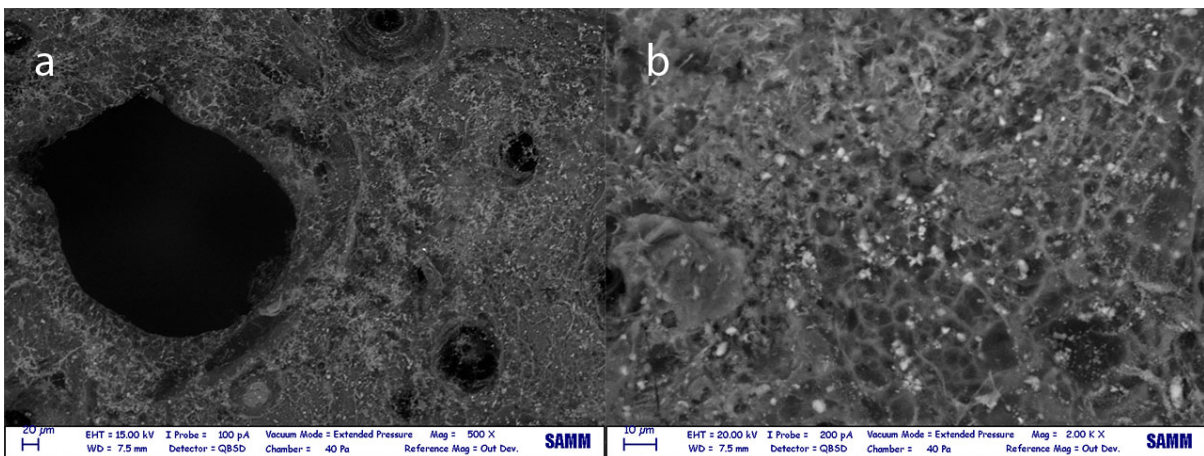
Figure 3-13: Backscattered SEM images at a)500x and b)2000x magnification for the 10% small grain size Bioglass samples prepared at pH 3.0 with square voltage (75-100V, 25-5s) after 20 min

It is noticeable that the homogeneity distribution of the Bioglass is the same also for the higher amount of Bioglass figure 3-14.
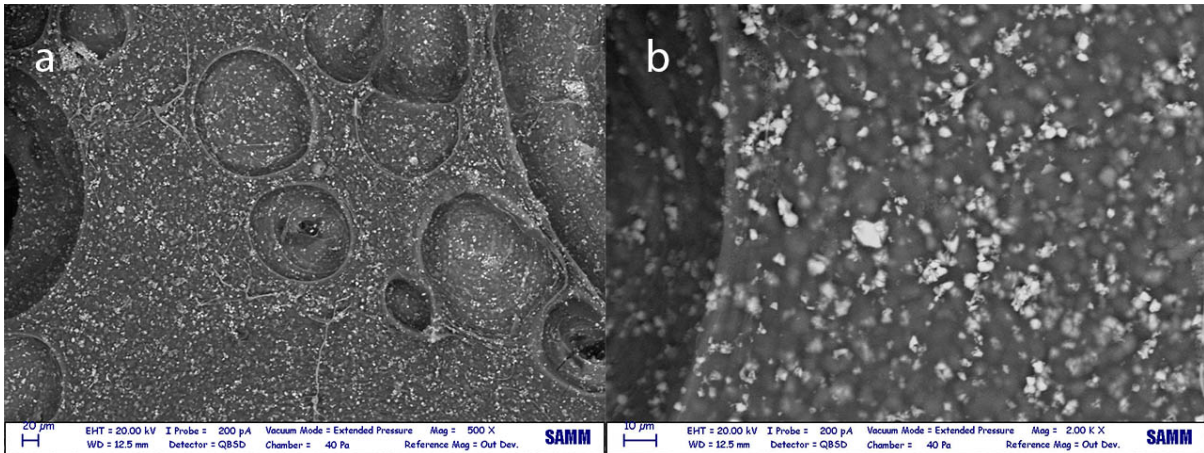
Figure 3-14: Backscattered SEM images at a)1000x and b)10,000x magnification for the solution contained 30% small grain size Bioglass samples prepared at pH 3.0 with square voltage (75-100V, 25-5s) after 20 min

For tissue engineering as bone transplant, the creation of a vascularized bed ensures the survival and function of seeded cells, which have access to the vascular system for nutrition, gas exchange, and elimination of by-products. The vascularization of a scaffold relying on capillary ingrowth into the interconnecting pore network from the host tissue. In situ, the distance between blood vessels and mesenchymal cells are not larger then 100 μm. Therefore, the time frame has to be taken into account for the capillary system to distribute through larger scaffold volume. It may also be possible to control the degree and rate of vascularization by incorporating angiogenic and anti-angiogenic factors in the degrading matrix of the scaffold [71].

Figure 3-15 shows the Haversian system or an osteon of compact bone. In mature, compact bone most of the individual lamellae form concentric rings around larger longitudinal canals (approx. 50 μm in diameter) within the bone tissue. These canals are called Haversian canals. Haversian canals typically run parallel to the surface and

along the long axis of the bone. A Haversian canal generally contains one or two capillaries and nerve fibers [79].
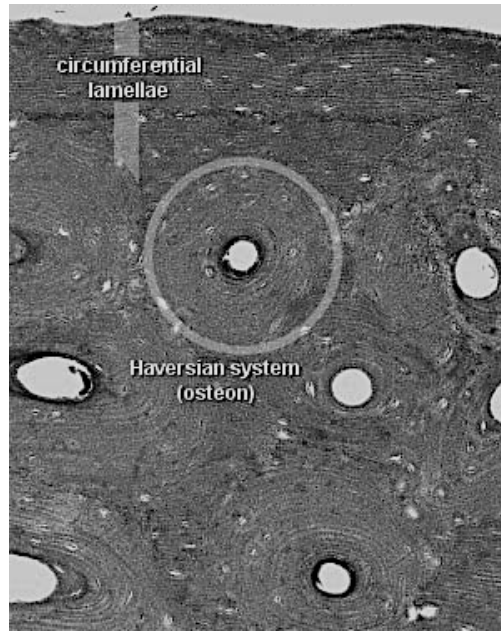
Figure 3-15: Haversian systems and interstitial lamellae

According to all mentioned factors, and similarities between fabricated CH-10BGL-P and CH-30BGS-P scaffolds and of bone's Haversian systems architecture showed in figure 3-16, one can conclude that by tuning the EPD parameters and using oriented porous patterned substrates as cathode it is possible to mimic compact bone structure.
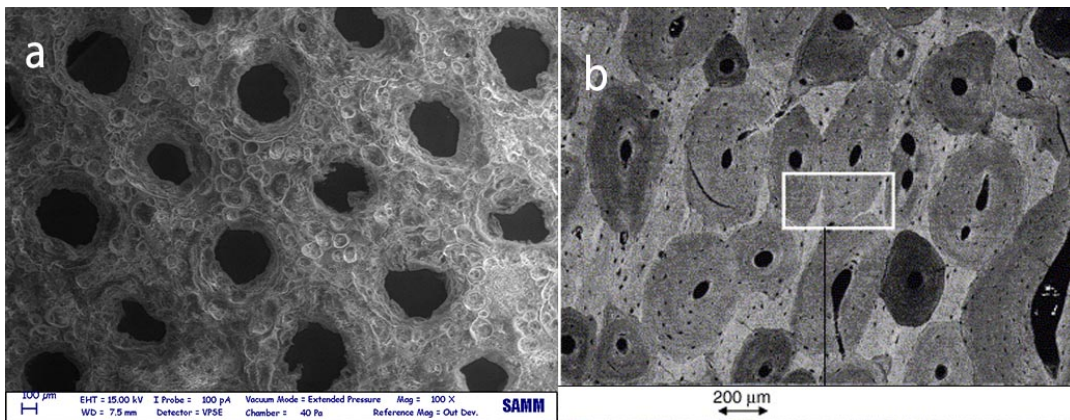
Figure 3-16: Compression between a) fabricated CH-30BGS-P sample with b) SEM image of Haversian system [80]

Shor et al. could construct Polycaprolactone (PCL) and composite PCL/hydroxyapatite (PCL–HA) tissue scaffolds by precision extrusion deposition (PED) process. They show that patterned structure of composite of their scaffolds have 60% and 70% porosity and with pore sizes of 450 and 750 µm. In vitro cell-scaffolds interaction study which has carried out using primary fetal bovine osteoblasts proved that the matrix oriented along the pores making circular regions similar to natural bone's Haversian systems (figure 3-17) [81].
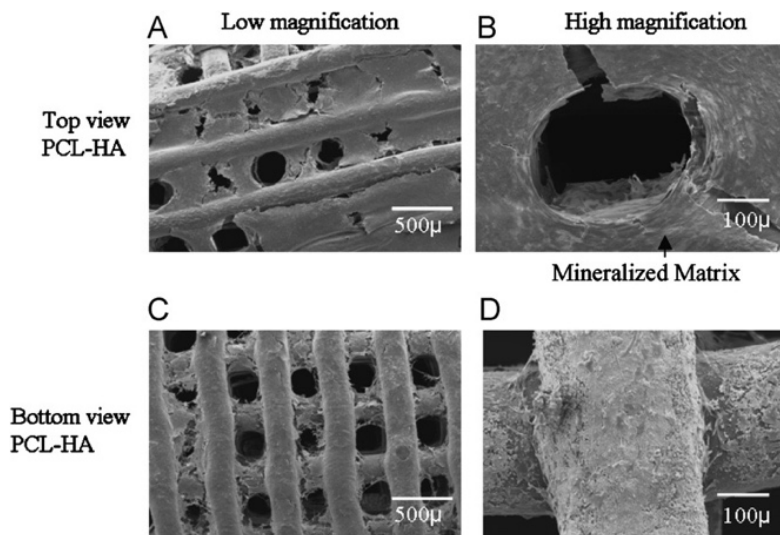
Figure 3-17: Scanning electron microscopy images showing top (A, B) and bottom views (C, D) of mineralized matrix produced by osteoblasts cultured on PCL–HA scaffolds after 21 days of culture [81].

3.4. Study the response of samples in SBF and PBS

For each of 7 sample families, based on the Table 2-4, 6 were prepared, three of which in SBF and three in PBS solutions.

ANOVA grouping of the electrodeposited samples are listed in Table 3-2. All the samples were prepared in square voltage mode (25seconds in Voltage 75V-, 5seconds in 100V). The final pH of all solution were adjusted by acetic acid to 3.0.

Table 3-2: ANOVA grouping of each sample family

Sample	ANOVA Grouping
CH	A
CH-10BGS	B
CH-10BGL	C
CH-30BGS	D

3.4.1. Water uptake and weight gain data

Water uptake percentage of patterned and non-patterned samples soaked in SBF and PBS are shown in Figure 3-18 to 3-21. Weight gain data is presented in Figures 3-22 to 3-25.
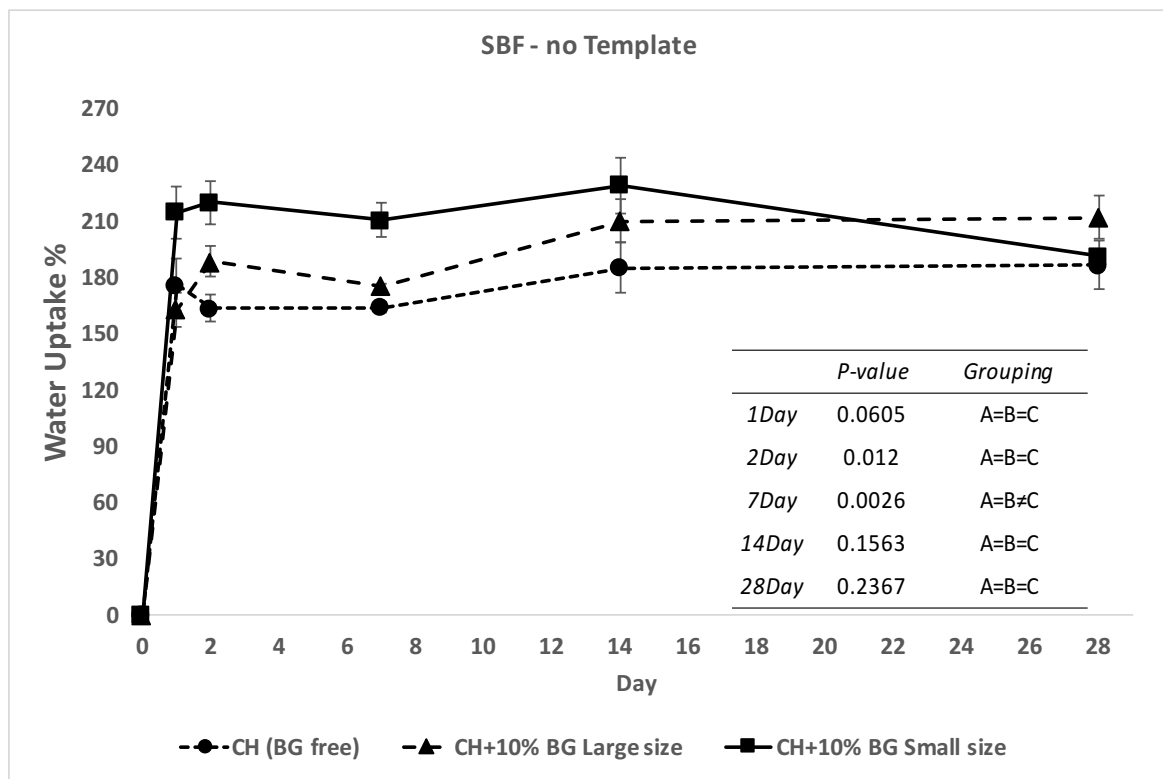
Figure 3-18: Water uptake percentages of non-patterned Bioglass free, samples with 10% large and small size Bioglass soaked in SBF up to 28 days.
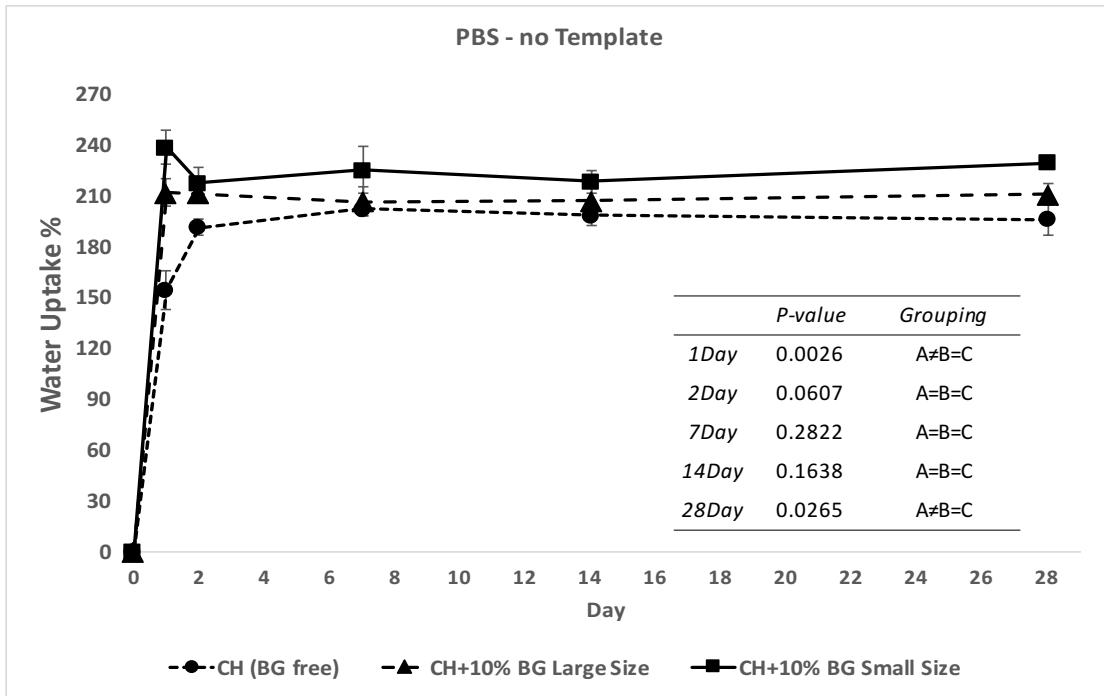
Figure 3-19: Water uptake percentages of non-patterned Bioglass free, samples with 10% large and small size Bioglass soaked in PBS up to 28 days
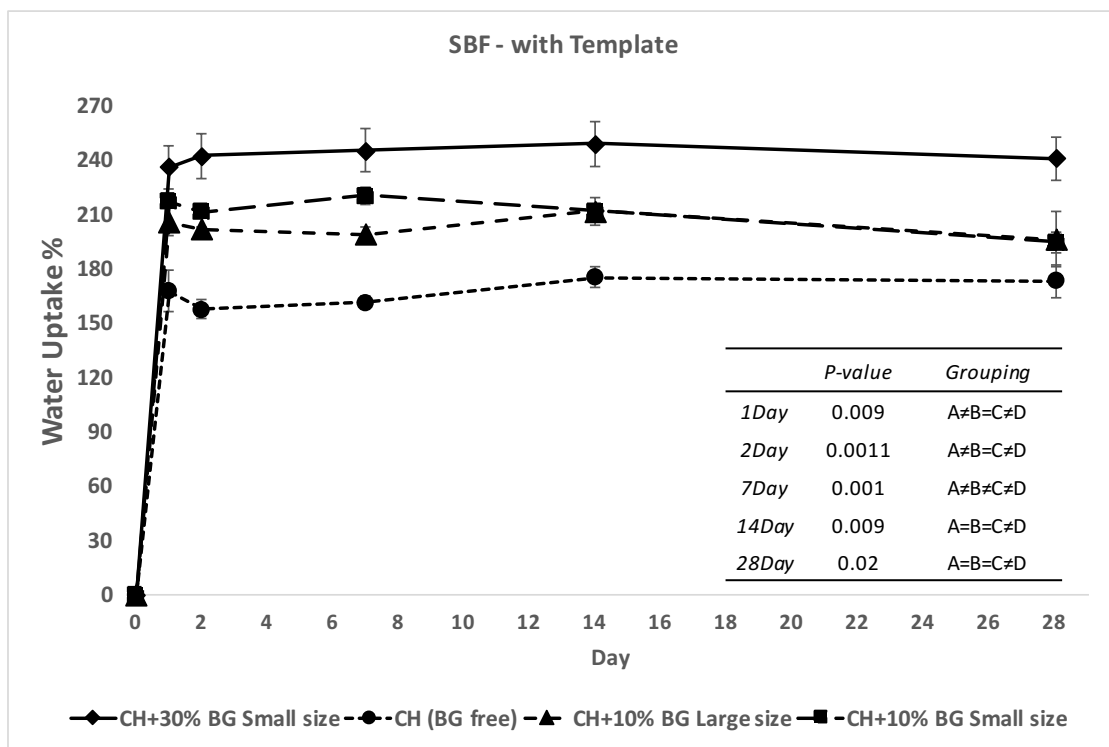
Figure 3-20: Water uptake percentages of patterned Bioglass free, samples with 10% large size Bioglass and 10% and 30% small size Bioglass soaked in SBF up to 28 days.
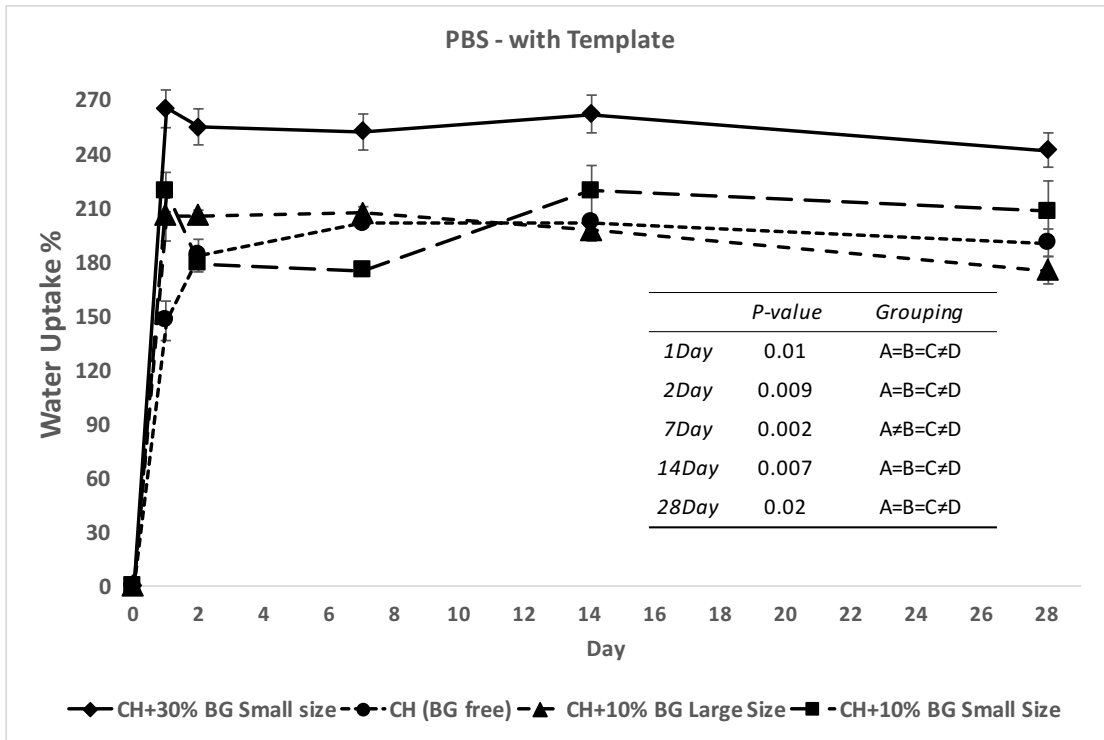
Figure 3-21: Water uptake percentages of patterned Bioglass free, samples with 10% large size Bioglass and 10% and 30% small size Bioglass soaked in PBS up to 28 days.
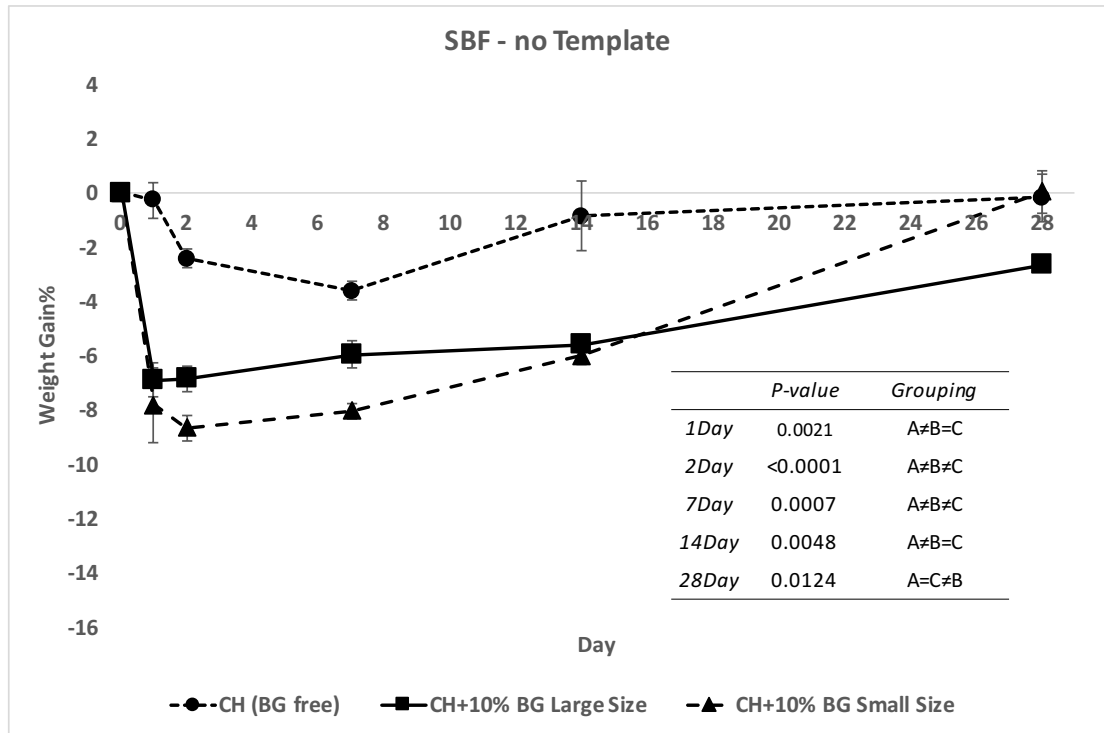
Figure 3-22: Weight gain percentage of non-patterned Bioglass free, samples with 10% large and small size Bioglass soaked in SBF up to 28 days.

51
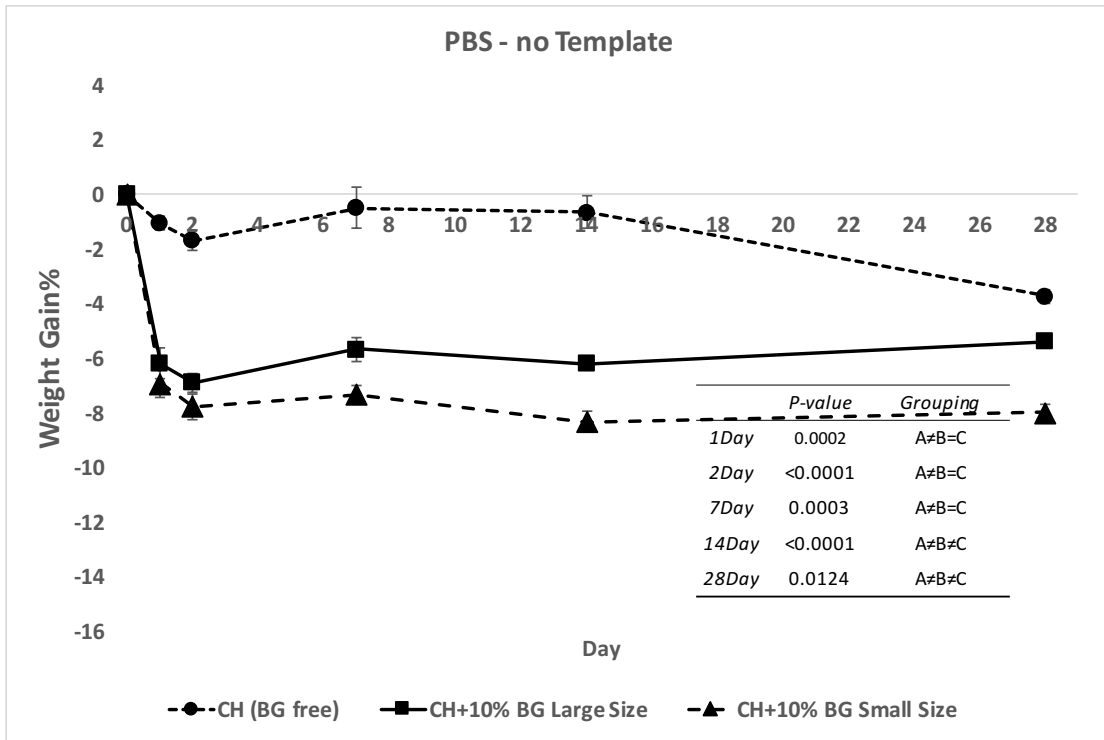
Figure 3-23: Weight gain percentage of non-patterned Bioglass free, samples with 10% large and small size Bioglass soaked in PBS up to 28 days.
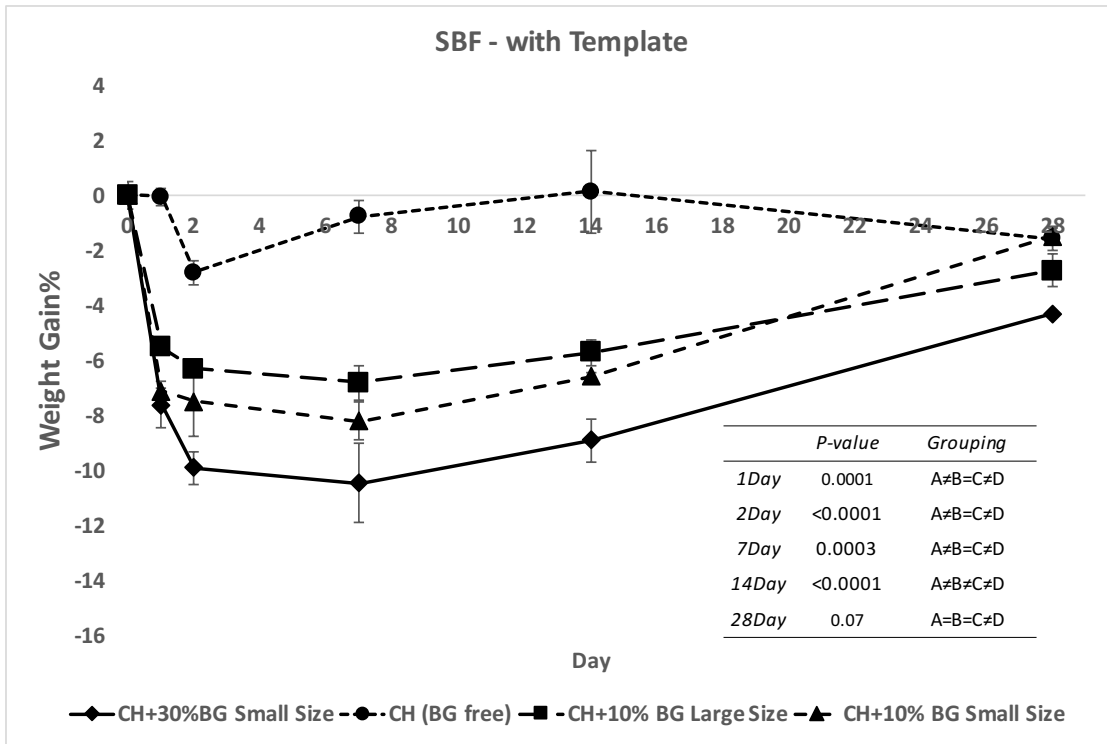
Figure 3-24: Weight gain percentages of patterned Bioglass free, samples with 10% large size Bioglass and 10% and 30% small size Bioglass soaked in SBF up to 28 days.
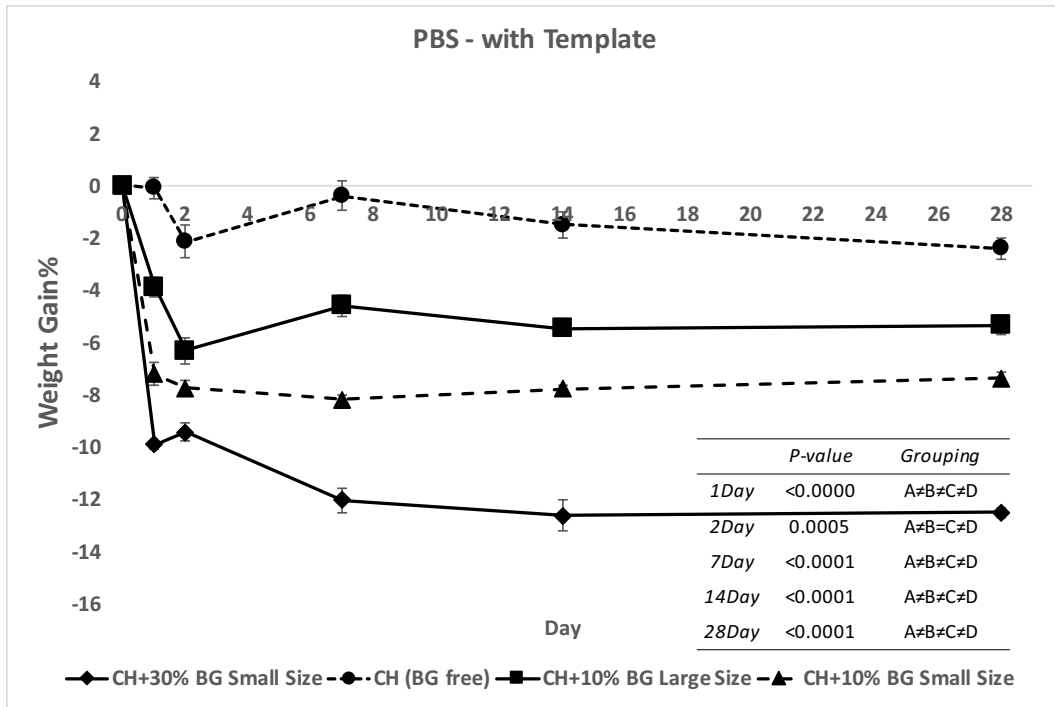
Figure 3-25: Weight gain percentages of patterned Bioglass free, samples with 10% large size Bioglass and 10% and 30% small size Bioglass soaked in PBS up to 28 days.

Chitosan is a weak base and is insoluble in water and organic solvent. However, it is soluble in dilute aqueous acidic solution (pH<6.5), which can convert glucosamine units into soluble form R–NH$_3^+$ [82]. Therefore, it is insoluble in both SBF and PBS, at pH 7.4. However, there should be a swelling when it is soaked it in SBF and PBS. Hydrophilicity of primary amidic (-CONH$_2$) group in structure of chitosan is the main reason of its tendency for high water absorption [83]. Any absorption, which causes a dimensional change, has potentially important clinical consequences. Furthermore, if the absorption also results in a significant generation of pressure, it can be damaging to the material and if the material is constrained within a cavity or is being used as a luting agent, can also be damaging to the associated restorative materials. On the other hand, some materials are required to promote the diffusion of water or aqueous solutions or specific drugs in order to achieve certain performance

requirements. Therefore, dimensional change over the time is an important parameter in choosing a biomaterial for tissue engineering [84].

According to water uptake graphs, one can identify that for both SBF and PBS after 2 days a saturation is reached. But more important point is that by increasing the Bioglass amount to 30% the water absorption is also increased. This fact is also confirmed by as Tukey's Honestly Significant Differences Test (D has different grouping with others). Details of ANOVA analysis is explained in appendix A. Marquet et al. also observed increase in water absorption for composite scaffold of porous poly(α-hydroxyacid)/Bioglass® due to hydrophilicity of Bioglass particles [40]. However, as ANOVA analysis shows, it is much harder to tell a difference in water uptake between small and large grain size samples from 10% Bioglass solution specially for patterned samples Figure 3-22 and 3-23.

As mentioned before, chitosan is insoluble in pH>6.5. Hence, weight gain or weight loss is a compromise of BG dissolution and calcium phosphate deposition on Bioglass particles.

These outcomes can be concluded from the weight gain data:

- There is almost zero dissolution of pure chitosan in both SBF and PBS at least up to 28 days,

- Because of chitosan insolubility, all weight changes are attributed to Bioglass dissolution or calcium phosphate deposition on samples from the solution through the mentioned mechanisms, explained in section 1.5.1,

- For all composite samples in PBS (Figure 3-23 and 3-25) there is a continuous dissolution of Bioglass in to the solution. But for the first days, dissolution is faster and then it reaches a constant value,

- In PBS, weight loss of samples contain small size Bioglass is higher than the large size Bioglass samples. It is also proven by the Tukey's data analysis in which these two data families (CH-10BGL and CH-10BGS) are related to different grouping. Moreover, weight loss is increased by increasing the amount of Bioglass, CH-30BGS samples has larger weight loss than the others. It is also clear by SEM image of the CH-30BGS-P samples in figure 3-26 obtained before and after 28 soaking in PBS. It is apparent that the most of BG particles dissolved after 28 days.
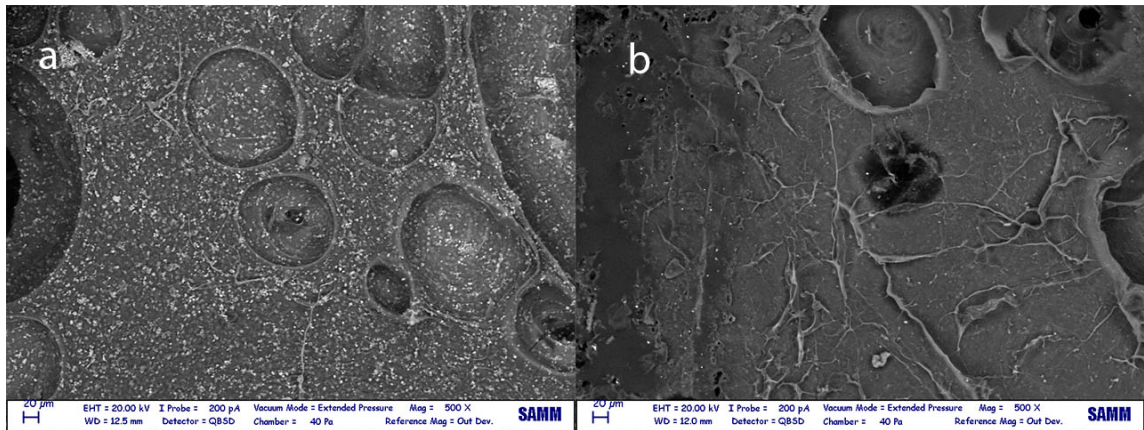
Figure 3-26: SEM images of CH-30BGS-P samples solution a) before and b) after 28 days soaking in PBS

- It is also confirmed by the EDS analysis of this sample shown in Table 3-3. All the elements except carbon and oxygen, which are from chitosan matrix, has values lower than 2 weight percent, which means that other elements has leached out from the composite during soaking for 28 days in PBS.

Table 3-3: EDS analysis of the sample CH+30%BG small size soaked 28 days in PBS WT%

Spectrum	C	O	Na	Al	Si	P	Cl	K	Ca	Total
CH+ 30% BG	50.41	45.44	0.19	1.26	0.08	1.29	0.60	0.00	0.73	100.00

Figure 3-22 and 3-24 display a compromise of two different phenomena; first, Bioglass dissolution until 7 days, and second, weight gains due to a calcium

phosphate phase deposition on the samples from SBF solution. From these graphs, one can see a drop in weight of all composite samples till day of 7 of soaking and then a slow weight increase until 28 days. This can be concluded that, up to 7 days, rate of Bioglass dissolution is higher than calcium phosphate deposition and after this time deposition rate is dominant.

According to elemental analysis represented in Table 3-3, there is also some amount of aluminum which is due to the of reaction of cathode substrate with acidic solution. Aluminum is an amphoteric element which is reactive in both high and low pHs. As can be seen in porbaix diagram of Al in figure 3-27, It is seen that Al is only nominally passive in the pH range of ~4 to 9 due to the presence of an Al_2O_3 film [85]. The deposition conditions for samples deposited in pH<4 was not as moderate as expected. As deposition on patterned substrates performed on pH=3.0, Al is not a good candidate for cathode metal.
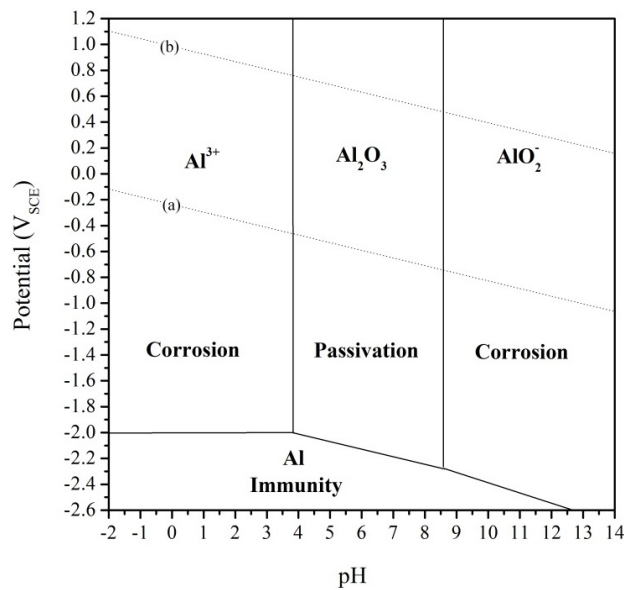
Figure 3-27: E-pH diagram for pure Al at 25˚C in aqueous solution (adapted from Pourbaix 1974). The lines (a) and (b) correspond to water stability and its decomposed product [85].

For eliminating Al if necessary there are different ways. For example, using lower voltage and longer time or using more corrosion resistance substrate such as stainless steel or platinum.

3.4.2. XRD analysis

To survey on possible deposited crystalline phases, XRD analysis was performed on some of the samples. Figure 3-28 shows the XRD graphs of the samples CH-30BGS in PBS for 7 and 28 days. As seen, there is no sharp peak which can be attribute to any crystalline phase. Wide peak at around $2\theta = 20°$ is probably for the amorphous chitosan matrix phase, because this peak was in XRD graphs of all other samples.
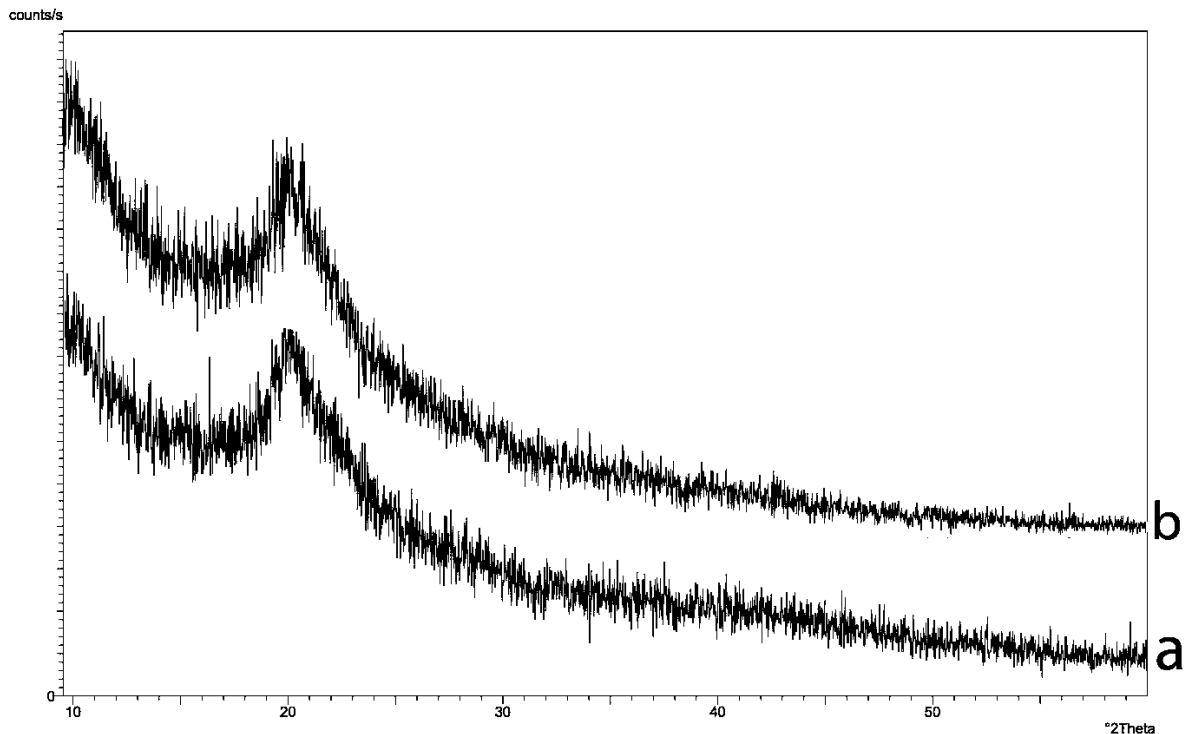
Figure 3-28: XRD pattern of CH+30% Bioglass small size samples soaked in PBS for a) 7days b) 28days

This confirms that PBS has not any effect on deposition of any calcium phosphate phase from Bioglass particles embedded in chitosan matrix. Bioglass particles gradually dissolve in PBS over time which was also confirmed by weight gain diagrams in Figures 3-23 and 3-25.

Figure 3-29 shows no significant peak for the samples soaked in SBF up to 7 days. But, for the samples of 14 and 28 days some sharp peaks start to appear which is attributed to a calcium phosphate dihydrate phase with formula $CaHPO_4.2H_2O$.
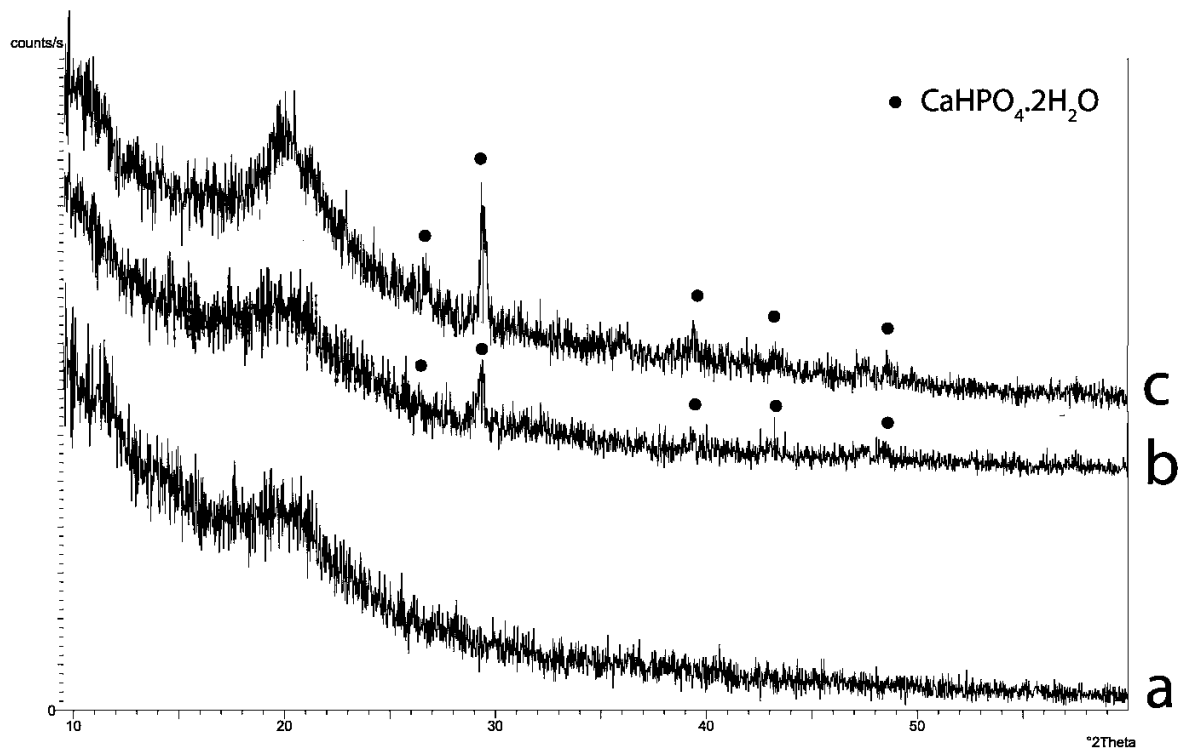
Figure 3-29: XRD pattern of CH+30BGS samples soaked in SBF for a) 7days b) 14days and c) 28days

First point that should be considered is that the height of the peak at $2\theta = 29.3°$ is increased during the time. This proves that amount of this calcium phosphate dihydrate phase increased over the time. Second, crystallization of calcium phosphate dihydrate phase shows in-vitro bioactivity of these samples. However, ratio of Ca/P of this phase is different from the Hydroxyapatite (HA), 1:1 instead of

5:3 for HA. This shows that the bioactivity of the samples in SBF was not as expected. In order to understand why the bioactivity decreased, EDS analysis of embedded Bioglass was measured to compare its composition with actual Bioglass 45S5®.

Table 3-3 shows the elemental analysis of the Bioglass 45S5® powder and sample deposited with this Bioglass.

Table 3-4: EDS analysis of Pure BG small size and sample CH+30% BG small size, all results in weight%

Spectrum	O	Na	Al	Si	P	K	Ca	Total
CH+30% BG small size	44.85	4.22	5.33	33.54	0.10	2.41	9.55	100.00
Pure BG 45S5®	46.55	12.60	0.00	19.58	2.09	0.01	19.17	100.00

As can be seen from Table 3-4, the amount of Sodium is reduced from 12.6 to 3.22 wt% and for Calcium it reduces from 19.17 to 9.55 wt%.

Because, there is the dissolution of modifier oxides of Bioglass (Na_2O and CaO) in to the solution even for the very first time of Bioglass addition to the solution. Figure 3-27 shows the dissolution percentage of Bioglass 45S5® with different particle sizes, up to 30 min [86].
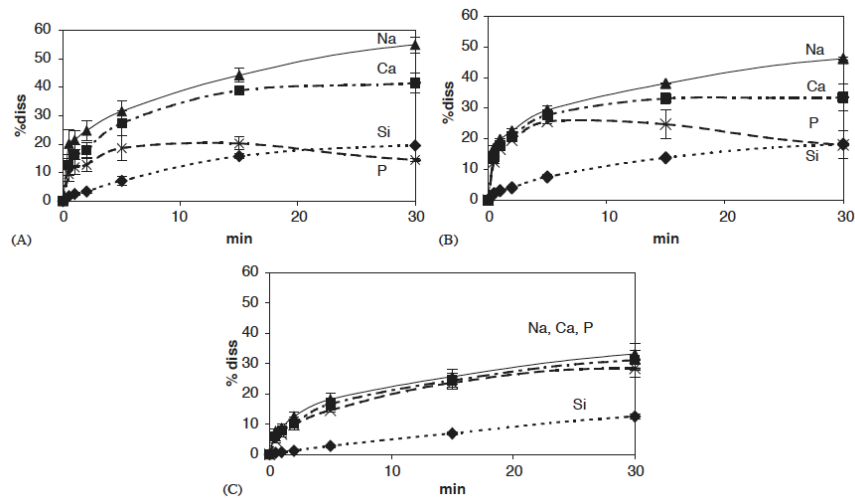
Figure 3-30: First 30 min dissolution of a Bioglass 45S5®with average particle size(A) 2μm, (B) 16μm, (C) 90μm Bioglass granulate samples in TRIS-buffered solutions .

The compositional dependence (in weight percent) of bone bonding and soft-tissue bonding for the Na_2O-CaO-P_2O_5-SiO_2 glasses has been explained by Hench [31] through a ternary phase diagram illustrated in Figure 3-31. All glasses in figure 3-31 contain a constant 6 wt% of P_2O_5. Compositions in the middle of the diagram (region A) form a bond with bone. Consequently, region A is termed the bioactive-bone-bonding boundary. Silica glasses within region B (such as window, bottle, or microscope slide glasses) behave as type 1, nearly inert materials and elicit a fibrous capsule at the implant-tissue interface. Glasses within region C are resorbable and disappear within 10 to 30 d of implantation. Glasses within region D are not technically practical and therefore have not been tested as implants.
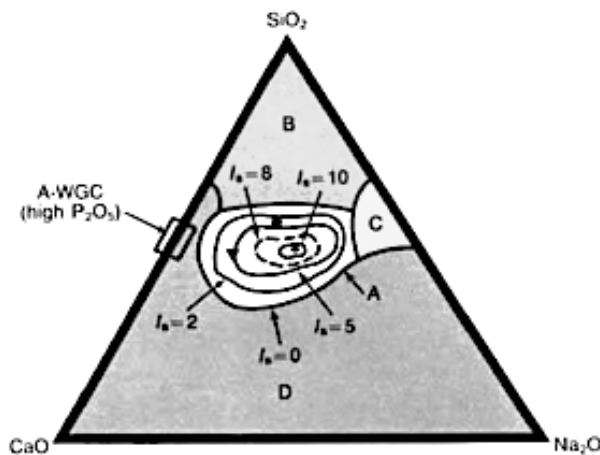
Figure 3-31: Compositional dependence (in weight percent) of bone bonding and soft-tissue bonding of bioactive glasses and glass- ceramics

According this diagram by dissolution of Na and Ca from the glass into the solution we go up to the apex of the triangle with less I_B. Therefore, this can be an explanation for formation of a calcium phosphate phase with Ca to P less than 5/3. This problem can be solved by reducing the dispersion time of Bioglass before deposition by using methods such as sonication or more strong mixing techniques, in order to reduce the the time for Bioglass particle dispersion.

3.4.3. pH analysis

The pH variation in different time intervals is shown in Figure 3-29 to 3-32.
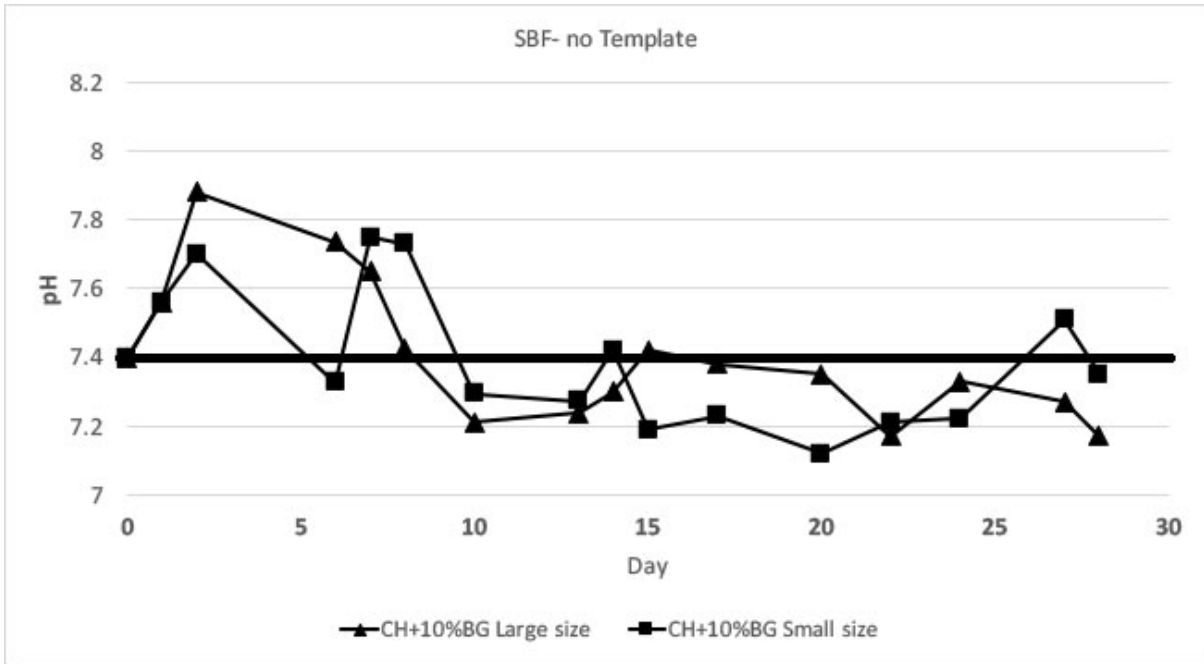
Figure 3-32: pH variation over the time intervals of SBF solution for non-patterned samples
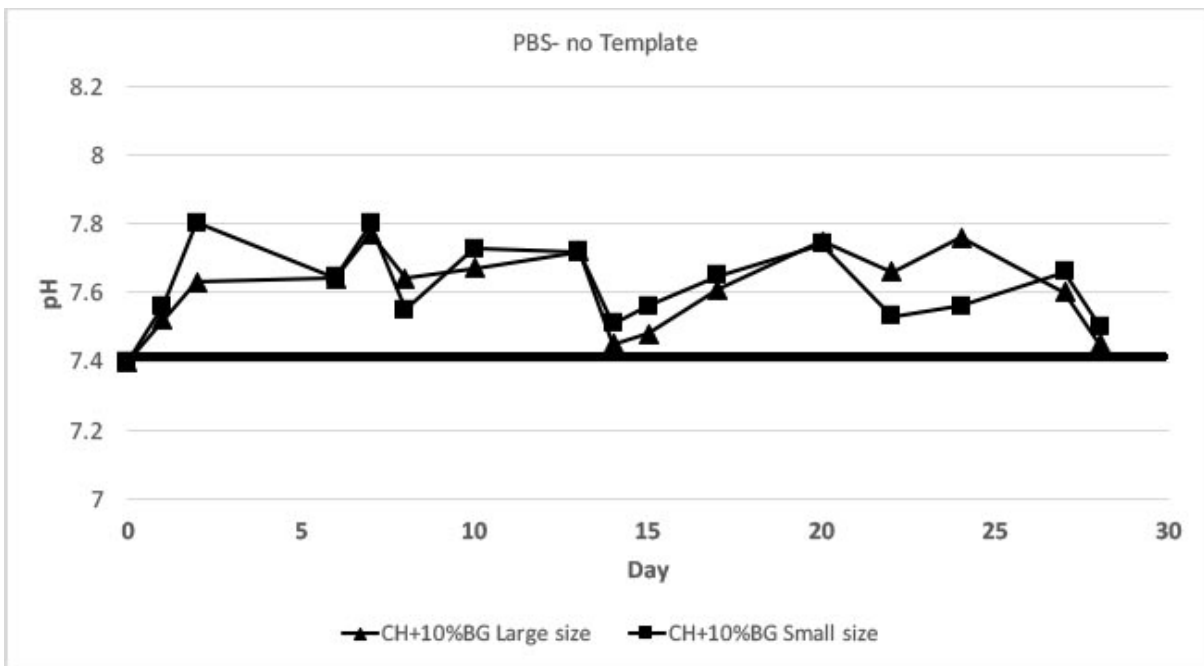
Figure 3-33: pH variation over the time intervals of PBS solution for non-patterned samples
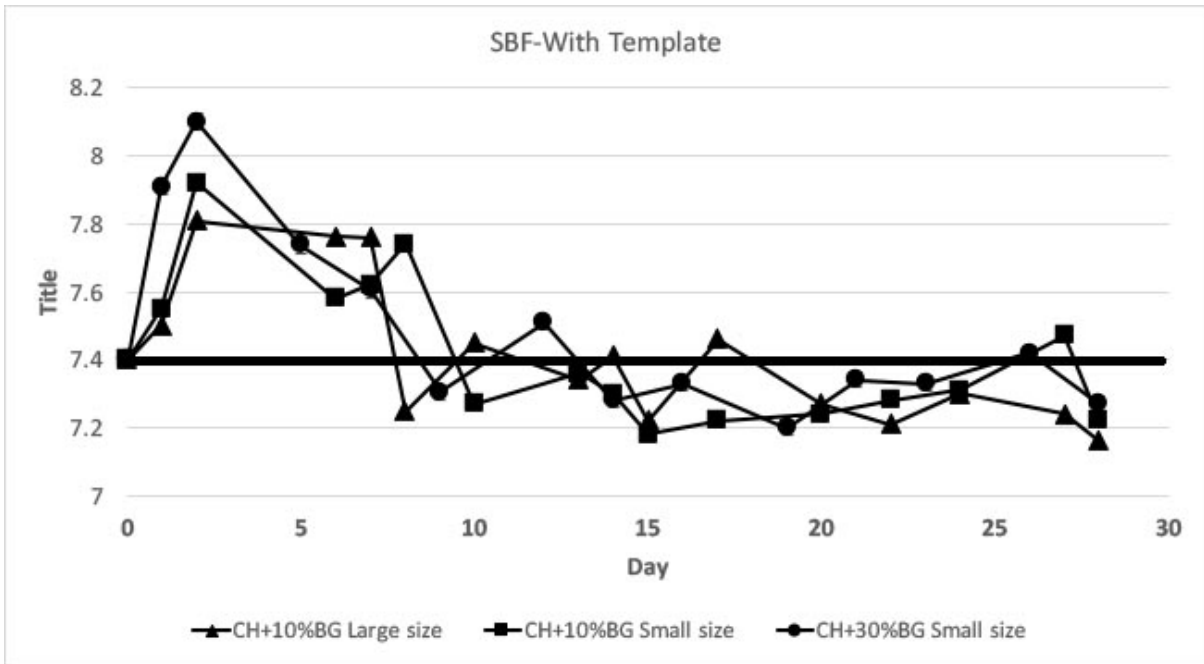
Figure 3-34: pH variation over the time intervals of SBF solution for patterned samples
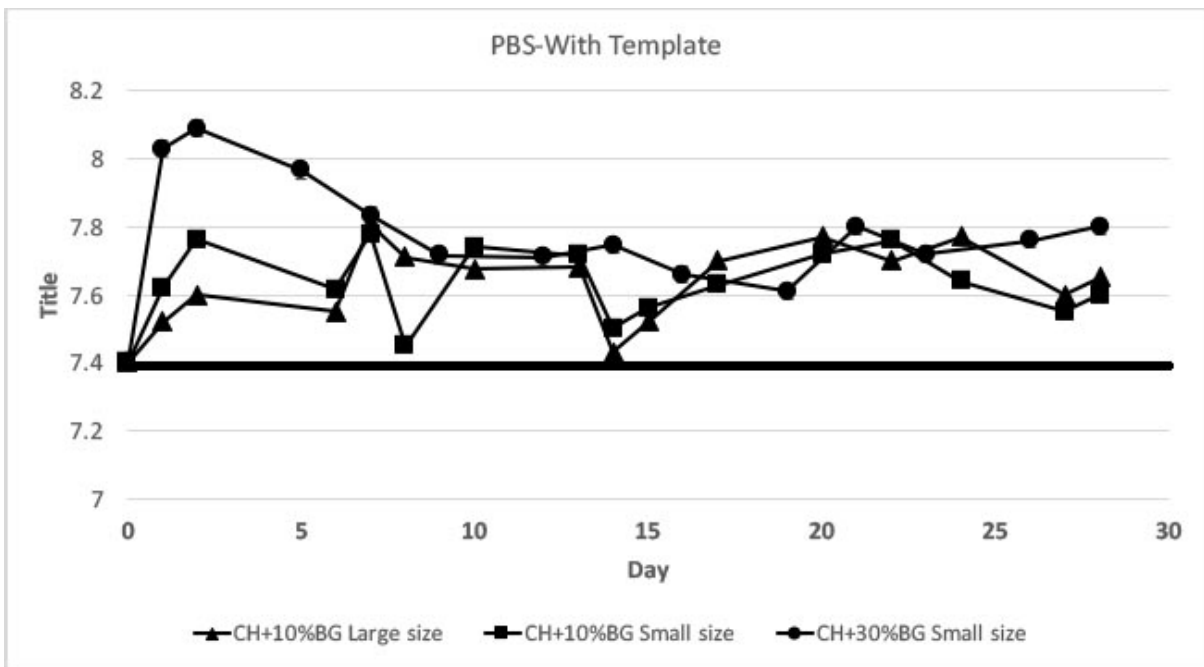
Figure 3-35: pH variation over the time intervals of PBS solution for patterned samples

pH of all PBS solutions are above initial value 7.4 for all time steps. It is because of continuous dissolution of the Bioglass into the solution and replacement of Na^+

and Ca^{2+} in the glass with H_3O^+ from the solution, which is consistent with weight gain data (Figure 3-23 and 3-25) and SEM (Figure 3-26) images. According to data from SBF solutions (Figure 3-34 and 3-32), there is shift in pH values after 7 days. All the pH data are placed below the initial value, pH<7.4 after 7 days. This change in pH can be attributed to the crystallization of calcium phosphate dihydrate which result in lowering of pH.

It is suggested that precipitation of calcium phosphate dihydrate is through following reaction[87]:

$$Ca^{2+} + H_2PO_4^{-2} + 3H_2O \rightarrow CaHPO_4.2H_2O + H_3O^+$$
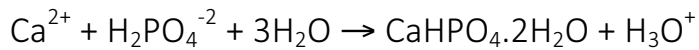
Production of H_3O^+ in this reaction is the main cause of pH reduction.

3.4.4. SEM-EDS analysis

Figure 3-33 shows the growth of calcium phosphate dihydrate in the SBF after 7, 14 and 28 days.

Figure 3-36: SEM images of CH+30% Bioglass small size at magnification 2000x after a) 7days, b) 14days, and c) 28days

As can be seen from Figure 3-33b, calcium phosphate dihydrate starts to grow and build up larger sites (Figure 3-33c). Although there is aggregation of calcium phosphate particles, homogeneity of deposition still holds (Figure 3-34).
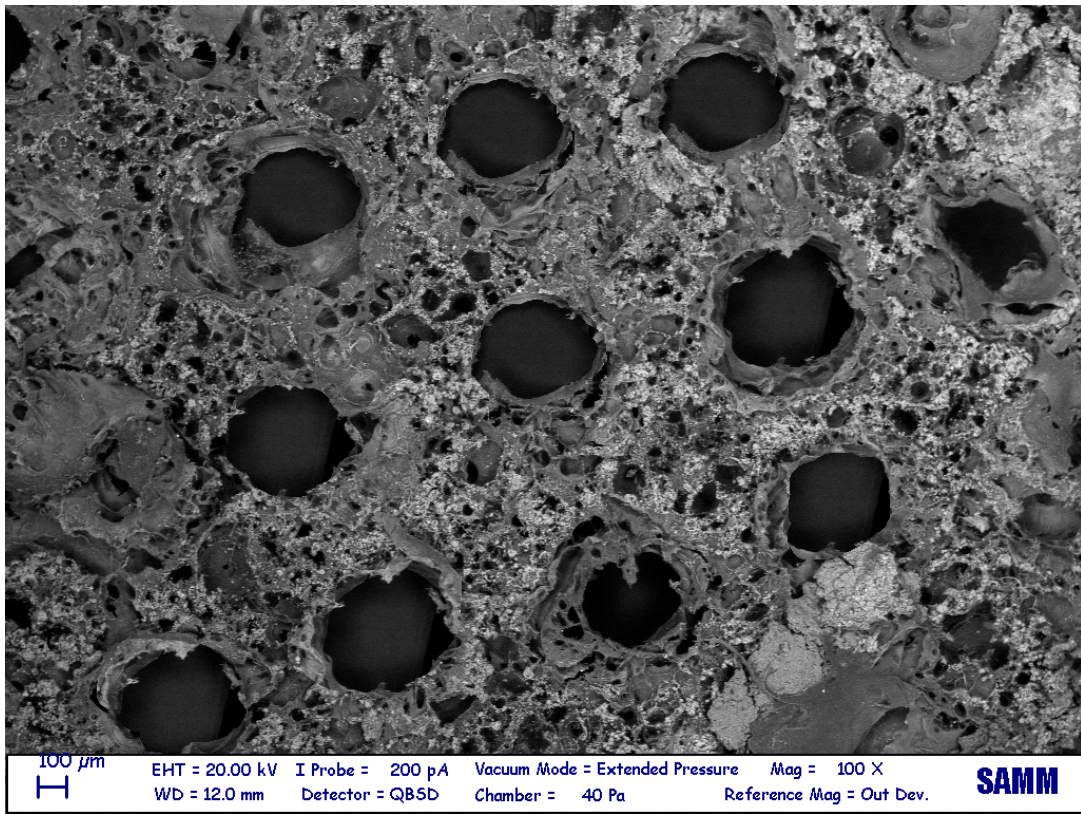
Figure 3-37: SEM images of CH+30% Bioglass small size at magnification 1000x after 28days

4. Conclusion and future directions

Electrophoretic deposition can be exploited to be used as a powerful rout for producing scaffolds with highly oriented porosities used in mimicking compact bone architecture. By changing parameters such as voltage, pH and Bioglass to chitosan ratio, scaffolds with homogeneously embedded Bioglass particles on patterned substrate with 500 μm pore size can be produced. In this regards, scaffolds with exact structure of target tissue (Harvesian system of compact bone in this case) can be formed to mimic the real functionality of composite biomaterials niche.

pH and conductivity has undeniable effect on the final quality of oriented micro channeled scaffolds.

Due to high rate of dissolution of the Bioglass particles, it is better to reduce the dispersion time before deposition.

BG particle increase water uptake of the composites in both SBF and PBS solutions.

Unlike SBF, PBS has no effect on calcium phosphate crystallization on the scaffolds.

Calcium phosphate dihydrate which is deposited in SBF solution has Ca to P ratio lower than HA, which is supposedly due to dissolution of Bioglass particles before deposition in the solution during dispersion time.

For the material of cathode due to acidic environment of deposition it is suggested to use a high corrosion resistance metal such as stainless steel instead of aluminum.

Further direction

1. Reducing the dispersion time for BG and survey on the change in composition of deposited embedded BG particles

2. Using stainless steel instead of Al as substrate to eliminate Al impurities in the scaffolds

3. Investigation on cell-scaffold interaction using Bovine Fetal Serum (FBS)

4. Investigation on cell viability and proliferation using Alamar Blue assay, a flurometric indicator of cell metabolic activity.

5. Investigate on feasibility of polymer matrix to be used as carrier for the release of therapeutics and drugs at the implantation site.

Appendices

A. ANOVA analysis

A one-way ANOVA is used to compare the means of more than two independent groups.

A.1. Five Step Hypothesis Testing Procedure

A.1.1. Check any necessary assumptions and write null and alternative hypotheses.

To apply or perform a one−way ANOVA, certain assumptions (or conditions) need to exist. If any of the conditions are not satisfied, the results from the use of ANOVA techniques may be unreliable. The assumptions are:

Each sample is an independent random sample

The distribution of the response variable follows a normal distribution

The population variances are equal across responses for the group levels. This can be evaluated by using the following rule of thumb: if the largest sample standard deviation divided by the smallest sample standard deviation is not greater than two, then assume that the population variances are equal.

Given that you are comparing k independent groups, the null and alternative hypotheses are:

$H_{0}: \mu_1 = \mu_2 = \cdots = \mu_k$

$H_{a}:$ Not all $\mu_\cdot$ are equal

In other words, the null hypothesis is that at all of the groups' population means are equal. The alternative is that they are not all equal; there are at two population means that are not equal to one another.

A.1.1. Calculate an appropriate test statistic.

The one-way ANOVA uses an F test statistic.

Conceptually, the F statistic is a ratio:

$F=\frac{Between\;groups\;variability}{Within\;groups\;variability}$.

Numerically this translates to $F=\frac{MS_{Between}}{MS_{Within}}$. In other words, how much do individuals in different groups vary from one another over how much to individuals within groups vary from one another.

Statistical software will compute the F ratio and produce what is known as an The ANOVA source (table A-1), will give information about the variability between groups and within groups. The table below gives all of the formulas, but calculations is done by software.

Table A-1: Calculation procedure by software

Source	SS	df	MS	F
Between Groups (Factor)	$\sum_{k}n_k(\overline{x}_k-\overline{x}_\cdot)^2$	k-1	$\frac{SS_{Between}}{df_{Between}}$	$\frac{MS_{Between}}{MS_{Within}}$
Within Groups (Error)	$\sum_k \sum_i(x_{ik}-\overline{x}_k)^2$	n-k	$\frac{SS_{Within}}{df_{Within}}$	
Total	$\sum_k \sum_i(x_{ik}-\overline{x}_\cdot)^2$	n-1		

k = Number of groups (Note: MyStatLab uses the symbol g)

n = Total sample size (all groups combined)

n_k = Sample size of group k

$\overline{x}_k$ = Sample mean of group k

$\overline{x}_\cdot$ = Grand mean (i.e., mean for all groups combined)

SS = Sum of squares

MS = Mean square

df = Degrees of freedom

F = F-ratio (the test statistic) using reference tables with defined alpha-value

Table F   The F Distribution

$\alpha = .05$

df_D \ df_N	1	2	3	4	5	6	7	8	9	10
1	161.4	199.5	215.7	224.6	230.2	234.0	236.8	238.9	240.5	241.9
2	18.51	19.00	19.16	19.25	19.30	19.33	19.35	19.37	19.38	19.40
3	10.13	9.55	9.28	9.12	9.01	8.94	8.89	8.85	8.81	8.79
4	7.71	6.94	6.59	6.39	6.26	6.16	6.09	6.04	6.00	5.96
5	6.61	5.79	5.41	5.19	5.05	4.95	4.88	4.82	4.77	4.74
6	5.99	5.14	4.76	4.53	4.39	4.28	4.21	4.15	4.10	4.06
7	5.59	4.74	4.35	4.12	3.97	3.87	3.79	3.73	3.68	3.64
8	5.32	4.46	4.07	3.84	3.69	3.58	3.50	3.44	3.39	3.35
9	5.12	4.26	3.86	3.63	3.48	3.37	3.29	3.23	3.18	3.14
10	4.96	4.10	3.71	3.48	3.33	3.22	3.14	3.07	3.02	2.98
11	4.84	3.98	3.59	3.36	3.20	3.09	3.01	2.95	2.90	2.85
12	4.75	3.89	3.49	3.26	3.11	3.00	2.91	2.85	2.80	2.75
13	4.67	3.81	3.41	3.18	3.03	2.92	2.83	2.77	2.71	2.67
14	4.60	3.74	3.34	3.11	2.96	2.85	2.76	2.70	2.65	2.60
15	4.54	3.68	3.29	3.06	2.90	2.79	2.71	2.64	2.59	2.54
16	4.49	3.63	3.24	3.01	2.85	2.74	2.66	2.59	2.54	2.49
17	4.45	3.59	3.20	2.96	2.81	2.70	2.61	2.55	2.49	2.45
18	4.41	3.55	3.16	2.93	2.77	2.66	2.58	2.51	2.46	2.41
19	4.38	3.52	3.13	2.90	2.74	2.63	2.54	2.48	2.42	2.38
20	4.35	3.49	3.10	2.87	2.71	2.60	2.51	2.45	2.39	2.35
21	4.32	3.47	3.07	2.84	2.68	2.57	2.49	2.42	2.37	2.32
22	4.30	3.44	3.05	2.82	2.66	2.55	2.46	2.40	2.34	2.30
23	4.28	3.42	3.03	2.80	2.64	2.53	2.44	2.37	2.32	2.27
24	4.26	3.40	3.01	2.78	2.62	2.51	2.42	2.36	2.30	2.25
25	4.24	3.39	2.99	2.76	2.60	2.49	2.40	2.34	2.28	2.24
26	4.23	3.37	2.98	2.74	2.59	2.47	2.39	2.32	2.27	2.22
27	4.21	3.35	2.96	2.73	2.57	2.46	2.37	2.31	2.25	2.20
28	4.20	3.34	2.95	2.71	2.56	2.45	2.36	2.29	2.24	2.19
29	4.18	3.33	2.93	2.70	2.55	2.43	2.35	2.28	2.22	2.18
30	4.17	3.32	2.92	2.69	2.53	2.42	2.33	2.27	2.21	2.16
40	4.08	3.23	2.84	2.61	2.45	2.34	2.25	2.18	2.12	2.08
60	4.00	3.15	2.76	2.53	2.37	2.25	2.17	2.10	2.04	1.99
120	3.92	3.07	2.68	2.45	2.29	2.17	2.09	2.02	1.96	1.91
∞	3.84	3.00	2.60	2.37	2.21	2.10	2.01	1.94	1.88	1.83

Figure A-1: F-Distribution for alpha=0.05

A.1.2. Determine a p-value associated with the test statistic.

When performing a one-way ANOVA using statistical software, there will be given the p-value in the ANOVA source table.

Normal F table is given for $\alpha=.05$, therefore you one only be able to determine if the p-value is less than or greater to .05. To read the F table, move horizontally to the correct df_1 and vertically to the correct df_2. Where this row and column intersect is the F value when $p=.05$. There is an inverse relationship between F and p. If your F statistic is less than this value then $p>.05$, if your F statistic is greater than this value then $p<.05$.

For example, let's say that you have an F test statistic of 3.98 with $df_1=3$ and $df_2=24$. Using the table we find, $F_{3, 24, .05}=3.01$. In other words, with 3 and 24 degrees of freedom, in order to be statistically significant at the 0.05 alpha level, an F test statistic of 3.01 or higher is needed. The F test statistic of 3.98 is greater than this value, therefore we know that $p<.05$ and the test is statistically significant.

A.1.3. Decide between the null and alternative hypotheses.

If $p \leq \alpha$ reject the null hypothesis. If $p>\alpha$ fail to reject the null hypothesis.

A.1.4. State a "real world" conclusion.

Based on your decision in step 4, write a conclusion in terms of the original research question.

A.2. Pairwise Comparisons

One-way ANOVAs are omnibus tests. This means that they provide information about the explanatory variable overall. While the results of a one-way ANOVA will tell us if there is what is known as a main effect of the explanatory variable, the initial results will not tell you which groups are different from one another. In order to determine which groups are different from one another, a post-hoc test is needed. Post-hoc tests are conduced after a one-way ANOVA to determine more precisely which groups differ. There are many different post-hoc analyses that could be performed following a one-way ANOVA. The most common tests known as Tukey's Honestly Significant Differences Test.

The theory behind this test is not given here and only show by total solve of one the analysis performed on weight gain after 28days PBS non-patterned samples using Minitab software:

A.3. One-Way ANOVA Minitab® software output

One-Way ANOVA: CH, non-patterned, PBS, 28D, CH + 10%BG Large size, non-patterned, CH + 10% BG Small size non-patterned, PBS, 28D

Method

Null hypothesis	H0: All means are equal
Alternative hypothesis	H1: At least one mean is different

Equal variances were assumed for the analysis.

Table A-2: Factor Information

Factor	Levels	Values
Factor	3	CH, non-patterned, PBS, 28D
		CH + 10%BG Large size, non-patterned, PBS, 28D
		CH + 10% BG Small size non-patterned, PBS, 28D

71

Table A-3: Analysis of Variance

Source	Degree of Freedom	Adj SS	Adj MS	F-value	P-value
Factor	2	94.0983	47.0492	93.30	<0.0001
Error	6	3.0256	0.5043		
Total	8	97.1240			

Table A-4: Model Summary

S	R-sq	R-sq(adj)	R-sq(pred)
0.710122	96.88%	95.85%	92.99%

Table A-5: Means

Fatcor	Number	Mean	Standard Deviation	95% confidence intervals
CH, non-patterned, PBS, 28D	3	-0.6491	1.0330	(-1.6523, 0.3541)
CH + 10%BG Large size, non-patterned, PBS, 28D	3	-6.2126	0.6392	(-7.2158, -5.2094)
CH + 10% BG Small size non-patterned, PBS, 28D	3	-8.3129	0.1930	(-9.3161, -7.3097)

Table A-6: Grouping Information Using the Tukey Method and 95% Confidence

Fatcor	Number	Mean	Grouping
CH, non-patterned, PBS, 28D	3	-0.6491	A
CH + 10%BG Large size, non-patterned, PBS, 28D	3	-6.2126	B
CH + 10% BG Small size non-patterned, PBS, 28D	3	-8.3129	C

Means that do not share a letter are significantly different.

Table A-7: Tukey Simultaneous Tests for Differences of Means

Fatcor	Difference of Means	Mean	SE of Difference	95% confidence intervals	T-Value	Adjusted P-Value
CH + 10%BG Large size, non-patterned, PBS, 28D & CH, non-patterned, PBS, 28D	3	-0.6491	1.0330	(-7.3429, -3.7842)	-9.60	0.0002
CH + 10%BG Small size, non-patterned, PBS, 28D & CH, non-patterned, PBS, 28D	3	-6.2126	0.6392	(-9.4432, -5.8845	-13.22	<0.0001
CH + 10% BG Small size non-patterned, PBS, 28D & CH + 10%BG Large size, non-patterned, PBS, 28D	3	-8.3129	0.1930	(-3.8797, -0.3209))	-3.62	0.0257

Individual confidence level = 97.80%
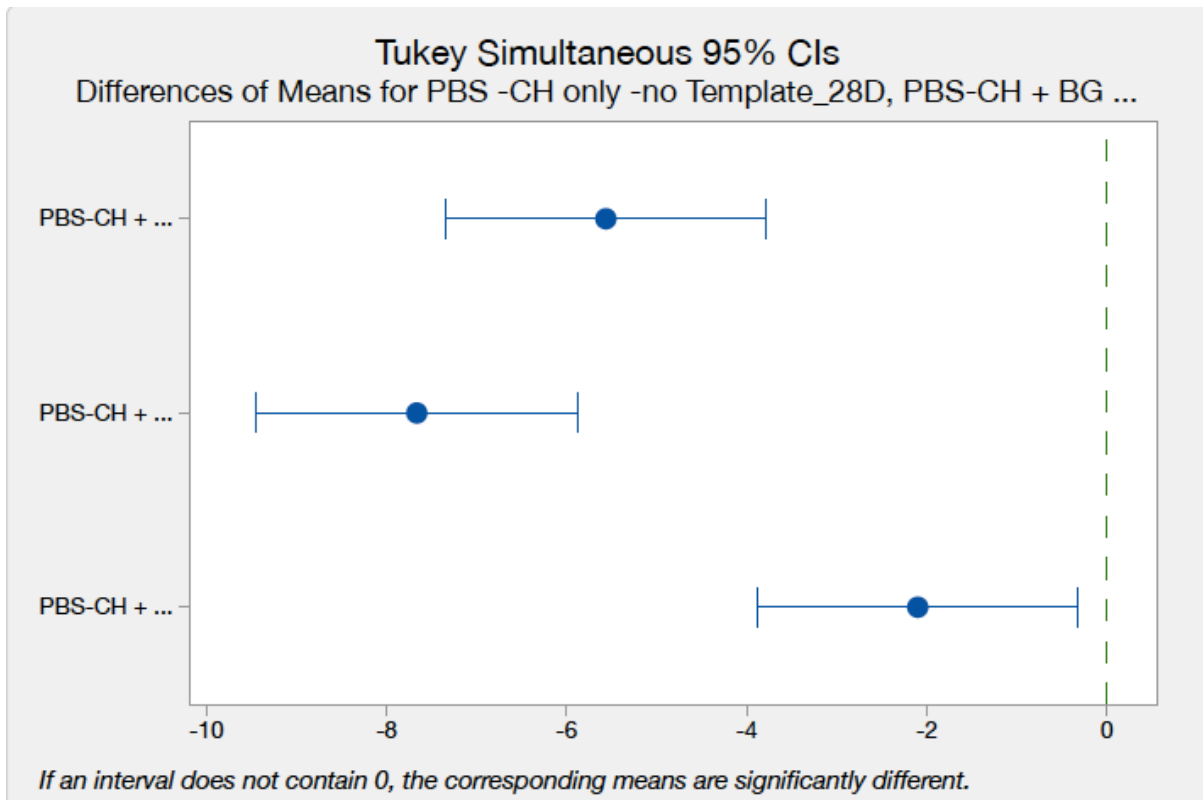
Figure A-2: Tukey Simultaneous 95% Confidence Intervals

Bibliography

[1]   M. E. Elsalanty and D. G. Genecov, "Bone Grafts in Craniofacial Surgery," *Cranial Maxillofac Trauma Reconstr.*, vol. 2, no. 03, pp. 125–134, 2009.

[2]   E. L. SCHELLER, P. H. KREBSBACH, and D. H. KOHN, "Tissue engineering: state of the art in oral rehabilitation," *J. Oral Rehabil.*, vol. 36, no. 5, pp. 368–389, 2009.

[3]   E. Neovius and T. Engstrand, "Craniofacial reconstruction with bone and biomaterials: Review over the last 11 years," *J. Plast. Reconstr. Aesthetic Surg.*, vol. 63, no. 10, pp. 1615–1623, Oct. 2010.

[4]   K. D. Hankenson, M. Dishowitz, C. Gray, and M. Schenker, "Angiogenesis in bone regeneration," *Injury*, vol. 42, no. 6, pp. 556–561, Jun. 2011.

[5]   E. Salter, B. Goh, B. Hung, D. Hutton, N. Ghone, and W. L. Grayson, "Bone Tissue Engineering Bioreactors: A Role in the Clinic?," *Tissue Eng. Part B Rev.*, vol. 18, no. 1, pp. 62–75, 2012.

[6]   S. N. Khan, F. P. Cammisa Jr., H. S. Sandhu, A. D. Diwan, F. P. Girardi, and J. M. Lane, "The biology of bone grafting.," *J. Am. Acad. Orthop. Surg.*, vol. 13, no. 1, pp. 77–86, 2005.

[7]   L. G. Griffith and G. Naughton, "Tissue engineering - current challenges and expanding opportunities.," *Science*, vol. 295. pp. 1009–14, 2002.

[8]   S. D. McCullen, A. G. Y. Chow, and M. M. Stevens, "In vivo tissue engineering of musculoskeletal tissues," *Curr. Opin. Biotechnol.*, vol. 22, no. 5, pp. 715–720, Oct. 2011.

[9]   S. Bose, M. Roy, and A. Bandyopadhyay, "Recent advances in bone tissue

engineering scaffolds," *Trends Biotechnol.*, vol. 30, no. 10, pp. 546–554, Oct. 2012.

[10] P. V Giannoudis, H. Dinopoulos, and E. Tsiridis, "Bone substitutes: An update," *Injury*, vol. 36, no. 3, Supplement, pp. S20–S27, Nov. 2005.

[11] T. N. Vo, F. K. Kasper, and A. G. Mikos, "Strategies for controlled delivery of growth factors and cells for bone regeneration," *Adv. Drug Deliv. Rev.*, vol. 64, no. 12, pp. 1292–1309, Sep. 2012.

[12] G. J. Meijer, J. D. de Bruijn, R. Koole, and C. A. van Blitterswijk, "Cell based bone tissue engineering in jaw defects," *Biomaterials*, vol. 29, no. 21, pp. 3053–3061, Jul. 2008.

[13] W. L. Grayson, P.-H. G. Chao, D. Marolt, D. L. Kaplan, and G. Vunjak-Novakovic, "Engineering custom-designed osteochondral tissue grafts," *Trends Biotechnol.*, vol. 26, no. 4, pp. 181–189, Apr. 2008.

[14] H. Peterlik, P. Roschger, K. Klaushofer, and P. Fratzl, "From brittle to ductile fracture of bone," *Nat. Mater.*, vol. 5, no. 1, pp. 52–55, 2006.

[15] A. K. Nair, A. Gautieri, S.-W. Chang, and M. J. Buehler, "Molecular mechanics of mineralized collagen fibrils in bone," *Nat. Commun.*, vol. 4, p. 1724, 2013.

[16] C. Li, A.-K. Born, T. Schweizer, M. Zenobi-Wong, M. Cerruti, and R. Mezzenga, "Amyloid-Hydroxyapatite Bone Biomimetic Composites," *Adv. Mater.*, vol. 26, no. 20, pp. 3207–3212, 2014.

[17] S. Weiner and H. D. Wagner, "The material bone: structure-mechanical function relations," *Annu. Rev. Mater. Sci.*, vol. 28, no. 1, pp. 271–298, 1998.

[18] M. M. Stevens, "Biomaterials for bone tissue engineering," *Mater. today*, vol. 11, no. 5, pp. 18–25, 2008.

[19] E. M. Bueno and J. Glowacki, "Cell-free and cell-based approaches for bone

regeneration," *Nat Rev Rheumatol*, vol. 5, no. 12, pp. 685–697, Dec. 2009.

[20] S. J. Hollister, "Scaffold Design and Manufacturing: From Concept to Clinic," *Adv. Mater.*, vol. 21, no. 32–33, pp. 3330–3342, 2009.

[21] C. Mangano, A. Piattelli, A. Mangano, F. Mangano, A. Mangano, G. Iezzi, F. L. Borges, S. D'Avila, and J. A. Shibli, "Combining Scaffolds and Osteogenic Cells in Regenerative Bone Surgery: A Preliminary Histological Report in Human Maxillary Sinus Augmentation," *Clin. Implant Dent. Relat. Res.*, vol. 11, pp. e92–e102, 2009.

[22] Y. S. Shayesteh, A. Khojasteh, M. Soleimani, M. Alikhasi, A. Khoshzaban, and N. Ahmadbeigi, "Sinus augmentation using human mesenchymal stem cells loaded into a β-tricalcium phosphate/hydroxyapatite scaffold," *Oral Surgery, Oral Med. Oral Pathol. Oral Radiol. Endodontology*, vol. 106, no. 2, pp. 203–209, Aug. 2008.

[23] R. Quarto, M. Mastrogiacomo, R. Cancedda, S. M. Kutepov, V. Mukhachev, A. Lavroukov, E. Kon, and M. Marcacci, "Repair of Large Bone Defects with the Use of Autologous Bone Marrow Stromal Cells," *N. Engl. J. Med.*, vol. 344, no. 5, pp. 385–386, 2001.

[24] K. Rezwan, Q. Z. Chen, J. J. Blaker, and A. R. Boccaccini, "Biodegradable and bioactive porous polymer/inorganic composite scaffolds for bone tissue engineering," *Biomaterials*, vol. 27, no. 18, pp. 3413–3431, 2006.

[25] L. L. Hench and J. M. Polak, "Third-generation biomedical materials," *Science (80-.).*, vol. 295, no. 5557, pp. 1014–1017, 2002.

[26] J. P. Vacanti and R. Langer, "Tissue engineering: the design and fabrication of living replacement devices for surgical reconstruction and transplantation," *Lancet*, vol. 354, pp. S32–S34, 1999.

[27] J. D. Kretlow, L. Klouda, and A. G. Mikos, "Injectable matrices and scaffolds for drug delivery in tissue engineering," *Adv. Drug Deliv. Rev.*, vol. 59, no. 4, pp. 263–273, 2007.

[28] C. Z. Liu and J. T. Czernuszka, "Development of biodegradable scaffolds for tissue engineering: a perspective on emerging technology," *Mater. Sci. Technol.*, vol. 23, no. 4, pp. 379–391, 2007.

[29] G. Jell and M. M. Stevens, "Gene activation by bioactive glasses," *J. Mater. Sci. Mater. Med.*, vol. 17, no. 11, pp. 997–1002, 2006.

[30] O. Tsigkou, L. L. Hench, A. R. Boccaccini, J. M. Polak, and M. M. Stevens, "Enhanced differentiation and mineralization of human fetal osteoblasts on PDLLA containing Bioglass{\textregistered} composite films in the absence of osteogenic supplements," *J. Biomed. Mater. Res. Part A*, vol. 80, no. 4, pp. 837–851, 2007.

[31] L. L. Hench, "Bioceramics: from concept to clinic," *J. Am. Ceram. Soc.*, vol. 74, no. 7, pp. 1487–1510, 1991.

[32] E. A. EL-HAFIAN, E. S. Elgannoudi, A. Mainal, and A. H. B. I. N. YAHAYA, "Characterization of chitosan in acetic acid: Rheological and thermal studies," *Turkish J. Chem.*, vol. 34, no. 1, pp. 47–56, 2010.

[33] I. M. El-Sherbiny and M. H. Yacoub, "Hydrogel scaffolds for tissue engineering: Progress and challenges," *Glob. Cardiol. Sci. Pract.*, p. 38, 2013.

[34] Q. Z. Chen and A. R. Boccaccini, "Poly (D, L-lactic acid) coated 45S5 Bioglass{\textregistered}-based scaffolds: Processing and characterization," *J. Biomed. Mater. Res. Part A*, vol. 77, no. 3, pp. 445–457, 2006.

[35] S. Ramakrishna, J. Mayer, E. Wintermantel, and K. W. Leong, "Biomedical applications of polymer-composite materials: a review," *Compos. Sci. Technol.*,

vol. 61, no. 9, pp. 1189–1224, 2001.

[36] M. Wang, "Developing bioactive composite materials for tissue replacement," *Biomaterials*, vol. 24, no. 13, pp. 2133–2151, 2003.

[37] R. M. Day, V. Maquet, A. R. Boccaccini, R. Jérôme, and A. Forbes, "In vitro and in vivo analysis of macroporous biodegradable poly (D, L-lactide-co-glycolide) scaffolds containing bioactive glass," *J. Biomed. Mater. Res. Part A*, vol. 75, no. 4, pp. 778–787, 2005.

[38] T. Jaakkola, J. Rich, T. Tirri, T. Närhi, M. Jokinen, J. Seppälä, and A. Yli-Urpo, "In vitro Ca-P precipitation on biodegradable thermoplastic composite of poly (\varepsilon-caprolactone-co-DL-lactide) and bioactive glass (S53P4)," *Biomaterials*, vol. 25, no. 4, pp. 575–581, 2004.

[39] J. J. Blaker, V. Maquet, R. Jérôme, A. R. Boccaccini, and S. N. Nazhat, "Mechanical properties of highly porous PDLLA/Bioglass® composite foams as scaffolds for bone tissue engineering," *Acta Biomater.*, vol. 1, no. 6, pp. 643–652, 2005.

[40] V. Maquet, A. R. Boccaccini, L. Pravata, I. Notingher, and R. Jérôme, "Porous poly (α-hydroxyacid)/Bioglass{\textregistered} composite scaffolds for bone tissue engineering. I: preparation and in vitro characterisation," *Biomaterials*, vol. 25, no. 18, pp. 4185–4194, 2004.

[41] A. R. Boccaccini and V. Maquet, "Bioresorbable and bioactive polymer/Bioglass® composites with tailored pore structure for tissue engineering applications," *Compos. Sci. Technol.*, vol. 63, no. 16, pp. 2417–2429, 2003.

[42] S. Deville, E. Saiz, and A. P. Tomsia, "Freeze casting of hydroxyapatite scaffolds for bone tissue engineering," *Biomaterials*, vol. 27, no. 32, pp. 5480–5489,

2006.

[43] V. S. Komlev, S. M. Barinov, and F. Rustichelli, "Strength enhancement of porous hydroxyapatite ceramics by polymer impregnation," *J. Mater. Sci. Lett.*, vol. 22, no. 17, pp. 1215–1217, 2003.

[44] D. M. Yunos, O. Bretcanu, and A. R. Boccaccini, "Polymer-bioceramic composites for tissue engineering scaffolds," *J. Mater. Sci.*, vol. 43, no. 13, pp. 4433–4442, 2008.

[45] X. Miao, L.-P. Tan, L.-S. Tan, and X. Huang, "Porous calcium phosphate ceramics modified with PLGA–bioactive glass," *Mater. Sci. Eng. C*, vol. 27, no. 2, pp. 274–279, 2007.

[46] T. Fukasawa, Z.-Y. Deng, M. Ando, T. Ohji, and Y. Goto, "Pore structure of porous ceramics synthesized from water-based slurry by freeze-dry process," *J. Mater. Sci.*, vol. 36, no. 10, pp. 2523–2527, 2001.

[47] H.-W. Kang, Y. Tabata, and Y. Ikada, "Fabrication of porous gelatin scaffolds for tissue engineering," *Biomaterials*, vol. 20, no. 14, pp. 1339–1344, 1999.

[48] N. Sultana and M. Wang, "PHBV/PLLA-based composite scaffolds fabricated using an emulsion freezing/freeze-drying technique for bone tissue engineering: surface modification and in vitro biological evaluation," *Biofabrication*, vol. 4, no. 1, p. 15003, 2012.

[49] I. Gill, "Bio-doped nanocomposite polymers: sol-gel bioencapsulates," *Chem. Mater.*, vol. 13, no. 10, pp. 3404–3421, 2001.

[50] P. Sepulveda, J. R. Jones, and L. L. Hench, "Bioactive sol-gel foams for tissue repair," *J. Biomed. Mater. Res.*, vol. 59, no. 2, pp. 340–348, 2002.

[51] Y. Wang, C. Yang, X. Chen, and N. Zhao, "Development and Characterization of Novel Biomimetic Composite Scaffolds Based on Bioglass-Collagen-Hyaluronic

Acid-Phosphatidylserine for Tissue Engineering Applications," *Macromol. Mater. Eng.*, vol. 291, no. 3, pp. 254–262, 2006.

[52] H. S. Mansur and H. S. Costa, "Nanostructured poly(vinyl alcohol)/bioactive glass and poly(vinyl alcohol)/chitosan/bioactive glass hybrid scaffolds for biomedical applications," *Chem. Eng. J.*, vol. 137, no. 1, pp. 72–83, 2008.

[53] J. A. Roether, A. R. Boccaccini, L. L. Hench, V. Maquet, S. Gautier, and R. Jérôme, "Development and in vitro characterisation of novel bioresorbable and bioactive composite materials based on polylactide foams and Bioglass® for tissue engineering applications," *Biomaterials*, vol. 23, no. 18, pp. 3871–3878, 2002.

[54] A. R. Boccaccini, A. G. Stamboulis, A. Rashid, and J. A. Roether, "Composite surgical sutures with bioactive glass coating," *J. Biomed. Mater. Res. Part B Appl. Biomater.*, vol. 67, no. 1, pp. 618–626, 2003.

[55] R. M. Day, A. R. Boccaccini, S. Shurey, J. A. Roether, A. Forbes, L. L. Hench, and S. M. Gabe, "Assessment of polyglycolic acid mesh and bioactive glass for soft-tissue engineering scaffolds," *Biomaterials*, vol. 25, no. 27, pp. 5857–5866, 2004.

[56] A. R. Boccaccini, S. Keim, R. Ma, Y. Li, and I. Zhitomirsky, "Electrophoretic deposition of biomaterials," *J. R. Soc. Interface*, vol. 7, no. Suppl 5, pp. S581–S613, 2010.

[57] P. Eiselt, J. Yeh, R. K. Latvala, L. D. Shea, and D. J. Mooney, "Porous carriers for biomedical applications based on alginate hydrogels," *Biomaterials*, vol. 21, no. 19, pp. 1921–1927, 2000.

[58] L. Besra and M. Liu, "A review on fundamentals and applications of electrophoretic deposition (EPD)," *Prog. Mater. Sci.*, vol. 52, no. 1, pp. 1–61,

2007.

[59] I. Corni, M. P. Ryan, and A. R. Boccaccini, "Electrophoretic deposition: from traditional ceramics to nanotechnology," *J. Eur. Ceram. Soc.*, vol. 28, no. 7, pp. 1353–1367, 2008.

[60] P. Sarkar and P. S. Nicholson, "Electrophoretic deposition (EPD): mechanisms, kinetics, and application to ceramics," *J. Am. Ceram. Soc.*, vol. 79, no. 8, pp. 1987–2002, 1996.

[61] R. N. Basu, C. A. Randall, and M. J. Mayo, "Fabrication of dense zirconia electrolyte films for tubular solid oxide fuel cells by electrophoretic deposition," *J. Am. Ceram. Soc.*, vol. 84, no. 1, pp. 33–40, 2001.

[62] T. Ishihara, K. Shimose, T. Kudo, H. Nishiguchi, T. Akbay, and Y. Takita, "Preparation of Yttria-Stabilized Zirconia Thin Films on Strontium-Doped LaMnO3 Cathode Substrates via Electrophoretic Deposition for Solid Oxide Fuel Cells," *J. Am. Ceram. Soc.*, vol. 83, no. 8, pp. 1921–1927, 2000.

[63] I. Zhitomirsky and A. Hashambhoy, "Chitosan-mediated electrosynthesis of organic–inorganic nanocomposites," *J. Mater. Process. Technol.*, vol. 191, no. 1, pp. 68–72, 2007.

[64] F. Pishbin, V. Mouriño, S. Flor, S. Kreppel, V. Salih, M. P. Ryan, and A. R. Boccaccini, "Electrophoretic deposition of gentamicin-loaded bioactive glass/chitosan composite coatings for orthopaedic implants," *ACS Appl. Mater. Interfaces*, vol. 6, no. 11, pp. 8796–8806, 2014.

[65] D. Zhitomirsky, J. A. Roether, A. R. Boccaccini, and I. Zhitomirsky, "Electrophoretic deposition of bioactive glass/polymer composite coatings with and without HA nanoparticle inclusions for biomedical applications," *J. Mater. Process. Technol.*, vol. 209, no. 4, pp. 1853–1860, 2009.

[66] C.-C. Yang, C.-C. Lin, and S.-K. Yen, "Electrochemical deposition of vancomycin/chitosan composite on Ti alloy," *J. Electrochem. Soc.*, vol. 158, no. 12, pp. E152–E158, 2011.

[67] K. D. Patel, R. K. Singh, E.-J. Lee, C.-M. Han, J.-E. Won, J. C. Knowles, and H.-W. Kim, "Tailoring solubility and drug release from electrophoretic deposited chitosan–gelatin films on titanium," *Surf. Coatings Technol.*, vol. 242, pp. 232–236, 2014.

[68] Y. Liu, W. Wang, G. Acharya, Y.-B. Shim, E. S. Choe, and C. H. Lee, "Advanced stent coating for drug delivery and in vivo biocompatibility," *J. nanoparticle Res.*, vol. 15, no. 10, pp. 1–16, 2013.

[69] M. M. Stevens, "Biomaterials for bone tissue engineering," *Mater. Today*, vol. 11, no. 5, pp. 18–25, 2008.

[70] M. J. Dalby, N. Gadegaard, R. Tare, A. Andar, M. O. Riehle, P. Herzyk, C. D. W. Wilkinson, and R. O. C. Oreffo, "The control of human mesenchymal cell differentiation using nanoscale symmetry and disorder," *Nat. Mater.*, vol. 6, no. 12, pp. 997–1003, 2007.

[71] D. W. Hutmacher, "Scaffolds in tissue engineering bone and cartilage," *Biomaterials*, vol. 21, no. 24, pp. 2529–2543, 2000.

[72] P. Bellatti and E. Brivio, "Cross-Linked Chitosan Patches for Topical Oral Drug Delivery," Politecnico di Milano, 2014.

[73] T. Kokubo, H. Kushitani, S. Sakka, T. Kitsugi, and T. Yamamuro, "Solutions able to reproduce in vivo surface-structure changes in bioactive glass-ceramic A-W3," *J. Biomed. Mater. Res.*, vol. 24, no. 6, pp. 721–734, 1990.

[74] T. Kokubo and H. Takadama, "How useful is SBF in predicting in vivo bone bioactivity?," *Biomaterials*, vol. 27, no. 15, pp. 2907–2915, 2006.

[75] Sigma-Aldrich, "General description." [Online]. Available: http://www.sigmaaldrich.com/catalog/product/sigma/p4417?lang=it&region =IT.

[76] a. Simchi, F. Pishbin, and a. R. Boccaccini, "Electrophoretic deposition of chitosan," *Mater. Lett.*, vol. 63, no. 26, pp. 2253–2256, 2009.

[77] I. Zhitomirsky and A. Hashambhoy, "Chitosan-mediated electrosynthesis of organic–inorganic nanocomposites," *J. Mater. Process. Technol.*, vol. 191, no. 1–3, pp. 68–72, 2007.

[78] I. Zhitomirsky, "Cathodic electrodeposition of ceramic and organoceramic materials. Fundamental aspects," *Adv. Colloid Interface Sci.*, vol. 97, no. 1, pp. 279–317, 2002.

[79] L. Slomianka, "Blue Histology - Skeletal Tissues - Bone," *School of Anatomy and Human Biology - The University of Western Australia*, 2009. [Online]. Available: http://www.lab.anhb.uwa.edu.au/mb140/corepages/bone/bone.htm.

[80] T. Hoc, L. Henry, M. Verdier, D. Aubry, L. Sedel, and A. Meunier, "Effect of microstructure on the mechanical properties of Haversian cortical bone," *Bone*, vol. 38, no. 4, pp. 466–474, 2006.

[81] L. Shor, S. Güçeri, X. Wen, M. Gandhi, and W. Sun, "Fabrication of three-dimensional polycaprolactone/hydroxyapatite tissue scaffolds and osteoblast-scaffold interactions in vitro," *Biomaterials*, vol. 28, no. 35, pp. 5291–5297, 2007.

[82] M. N. V. R. Kumar, R. Muzzarelli, C. Muzzarelli, H. Sashiwa, and A. J. Domb, "Chitosan chemistry and pharmaceutical perspectives," *Chem. Rev.*, vol. 104, no. 12, pp. 6017–6084, 2004.

[83] F. Ganji, S. Vasheghani-Farahani, and E. Vasheghani-Farahani, "Theoretical

description of hydrogel swelling: a review," *Iran Polym J*, vol. 19, no. 5, pp. 375–398, 2010.

[84] J. F. McCabe and S. Rusby, "Water absorption, dimensional change and radial pressure in resin matrix dental restorative materials," *Biomaterials*, vol. 25, no. 18, pp. 4001–4007, 2004.

[85] N. L. Sukiman, X. Zhou, N. Birbilis, A. E. Hughes, J. M. C. Mol, S. J. Garcia, X. Zhou, and G. E. Thompson, "Durability and Corrosion of Aluminium and Its Alloys: Overview, Property Space, Techniques and Developments," in *Aluminium Alloys - New Trends in Fabrication and Applications*, .

[86] M. G. Cerruti, D. Greenspan, and K. Powers, "An analytical model for the dissolution of different particle size samples of Bioglass® in TRIS-buffered solution," *Biomaterials*, vol. 26, no. 24, pp. 4903–4911, 2005.

[87] F. Barrere, C. A. Van Blitterswijk, K. De Groot, and P. Layrolle, "Influence of ionic strength and carbonate on the Ca-P coating formation from SBF× 5 solution," *Biomaterials*, vol. 23, no. 9, pp. 1921–1930, 2002.